

Investigations on Energy Optimal Solutions to Control a Forestry Crane

Master's Thesis of

cand. M.Sc. Tim Schulz

matriculation number: 1841576

at the Department of Mechanical Engineering
Institute of Vehicle System Technology
Institute of Mobile Machines

Advisor: Prof.Dr.-Ing. Marcus Geimer
Co-Advisor: M.Sc. Chris Geiger

01/15/2021 – 06/30/2021

Karlsruhe Institute of Technology
Department of Mechanical
Engineering Kaiserstraße 12
76131 Karlsruhe

Institut für Fahrzeugsystemtechnik (FAST)
Institutsteil Mobile Arbeitsmaschinen (Mobima)

Prof. Dr.-Ing. Marcus Geimer

Masterarbeit

Nr.: 21 – M – 0005

für Herrn *cand. mach. (BSc.)* Tim Schulz

Matrikel Nr.: 1841576

Untersuchungen zu energieoptimalen Lösungen für die Steuerung eines Forstkranes

Im vollmechanisierten Holzernteprozess werden die stehenden Bäume von Harvestern gefällt und aufgearbeitet. Anschließend werden die zugeschnittenen Stämme mit Forwardern aus der Einschlagsfläche zum Polterplatz gerückt. Ein automatisches Steuern der Kranspitze von Forstmaschinen bietet dabei ein Potential zur Reduktion des Energieverbrauchs während des Arbeitsprozesses.

Dazu sollen in dieser Abschlussarbeit das Potential der möglichen Energiereduktion für das im Forwarder verbaute Prototypen-Hydrauliksystem sowie eine steuerungstechnische Umsetzung dessen untersucht werden. Hierzu werden die Ansätze mittels einer gewichteten Pseudo-Inversen, mit optionaler Nullraumoptimierung der Kinematik, den auf Trajektorien basierenden Ansätzen gegenübergestellt und verglichen, wobei Anlehnungen in der Robotik gesucht werden. Die Lösungsmöglichkeit mit dem größten Potential wird steuerungstechnisch ausgearbeitet und mittels des Simulationsmodells des Arbeitsantriebes getestet und evaluiert.

Die Masterarbeit umfasst die folgenden Schritte:

- Recherche zum Stand der Technik und Forschung
- Ermittlung des möglichen Energieeinsparpotential in Bezug auf das verbaute HT-System
- Ausarbeitung und Evaluierung der Energiereduktion mittels einer Pseudo-Inverse
- Untersuchung der Energiereduktion mittels Trajektorien-basierte Ansätze
- Steuerungstechnische Ausarbeitung
- Einbindung in das Simulationsmodell des Arbeitsantriebes
- Evaluation der Energiereduktion im Referenzzyklus
- Schriftliche Dokumentation in Form einer wissenschaftlichen Arbeit
- Präsentation der gewonnenen Erkenntnisse in Form eines Vortrags mit Diskussion

Tag der Ausgabe: 15.01.2019

Co-Betreuer: M.Sc. Chris Geiger

- Prof. Dr.-Ing. Marcus Geimer –

KIT – Die Forschungsuniversität in der Helmholtz-Gemeinschaft www.kit.edu

I truthfully assure that I have made the thesis independently, that I have specified all resources used completely and accurately and that I have labeled everything that has been taken from the work of others, either unchanged or with amendments, as well as that I have observed the articles of KIT for the Assurance of Good Scientific Practice as amended from time to time.

Ich versichere wahrheitsgemäß, die Arbeit selbstständig angefertigt, alle benutzten Hilfsmittel vollständig und genau angegeben und alles kenntlich gemacht zu haben, was aus Arbeiten anderer unverändert oder mit Änderungen entnommen wurde sowie die Satzung des KIT zur Sicherung guter wissenschaftlicher Praxis in der jeweils gültigen Fassung beachtet zu haben.

Karlsruhe, 30. June 2021

.....
(cand. M.Sc. Tim Schulz)

iv

Abstract

Due to the progressing climate change, climate-neutral resources are becoming increasingly important. The forest industry is aware of this problem and hence, is looking for new technologies to make the production of its natural resource more efficient. Therefore, this thesis presents an energetic optimization of a forestry crane. For this purpose, a pseudoinverse solution of the crane kinematics is optimized by the gradient projection method according to minimum hydraulic pressure and flow rate. The hydraulic pressure reveals to be the relevant optimization parameter. By increasing the feedback pressure, its influence on high-pressure peaks is increased in order to successfully reduce these. To maximize the energy savings, a hydraulic transformer is included in this approach. By coupling the inner and outer boom, potential energy is utilized for contrary motions of these. The developed algorithm for optimizing the energy demand is implemented in a holistic simulation model of a forestry crane arm. The effectiveness of this approach is tested in the model using representative trajectories. Energy savings of up to 26.9 % compared to a least norm pseudoinverse solution can be determined using the optimized control system. When the energy-saving potential of the coupling of the inner and outer boom is also considered, the total reduction in energy increases to up to 31.8 %.

Keywords:

forwarder, knuckle-boom crane, energy optimization, gradient projection method

Kurzfassung

Durch den fortschreitenden Klimawandel gewinnen klimaneutrale Rohstoffe zunehmend an Bedeutung. Die Forstindustrie ist sich dieser Problematik bewusst und sucht nach neuen Technologien, um auch die Produktion ihres natürlichen Rohstoffes effizienter zu gestalten. Im Hinblick darauf präsentiert die vorliegende Arbeit eine energetische Optimierung eines Forstkrans. Dafür wird eine pseudoinverse Lösung der Kinkinematik mit Hilfe der Gradient Projection Method nach minimalem Hydraulikdruck und Volumenstrom optimiert. Dabei zeigt sich der Hydraulikdruck als maßgebliche Optimierungsgröße. Durch ein Potenzieren des Rückmeldedrucks wird dessen Einfluss auf Druckspitzen gesteigert, um diese erfolgreich zu reduzieren. Um die Energieeinsparung zu maximieren wird ein hydraulischer Transformator in diesen Ansatz mit eingebunden. Dabei wird durch eine Kopplung von Hub- und Wipparm potenzielle Energie bei gegenläufigen Bewegungen dieser genutzt. Der entwickelte Algorithmus zur Optimierung des Energiebedarfs wird in ein holistisches Simulationsmodell des Forstkrans implementiert. Die Effektivität dieses Ansatzes wird in dem Modell anhand von repräsentativen Trajektorien geprüft. Dabei kann eine Energieeinsparung von bis zu 26,9 %, gegenüber einer Least-Norm-Pseudoinversen-Lösung, durch die optimierte Steuerung ermittelt werden. Wenn man das Energiesparpotential der Kopplung von Hub- und Wipparm mit einbezieht, erhöht sich die Gesamtreduktion der Energie auf bis zu 31,8 %.

Schlüsselwörter:

Forwarder, Forstkran, Energieoptimierung, Gradient Projection Method

ii

Acknowledgements

Firstly, I would like to thank my advisor Chris Geiger for always supporting me during this thesis. Our weekly meetings and close interaction were a great benefit to the success of this thesis. Under the circumstances of the pandemic, this cannot be taken for granted. I have truly appreciated working together with you and I am very thankful for the time and effort you invested. Furthermore, I want to thank your whole team for always immediately supporting me with concerns and questions.

One more thank you goes to my friends, who supported me during this thesis, either by inspiring me with technical discussions or by advising me during the writing process. Even if I can't mention all of you, I will reciprocate your help and thank you in person for your support.

Finally, a big thank you goes to my family, who always supported me to reach the goals I aim for. It is wonderful that I can always rely on you!

iv

Contents

1 Introduction	1
1.1 Motivation	1
1.2 Scope of the Thesis	1
1.3 Outline	2
2 Fundamentals	3
2.1 Kinematics of Robotic Manipulators	3
2.1.1 Elementary Kinematics	4
2.1.2 Task Space and Conguration Space	6
2.1.3 Denavit-Hartenberg Parameters	7
2.1.4 Forward Kinematics	9
2.1.5 Inverse Kinematics	10
2.1.6 Trajectories	11
2.2 Load Sensing Hydraulic Systems	12
3 State of the Art	14
3.1 Technical Specifications of a Forwarder	14
3.1.1 Forwarder Design	14
3.1.2 Knuckle-Boom Crane	15
3.1.3 Energy Optimization of the Knuckle-Boom Crane	16
3.1.4 Energy Savings Through a Hydraulic Transformer	16
3.2 Presentation of Several Closed-Form and Numerical Solutions	18
4 Methods	26
4.1 Denavit Hartenberg Notation of the Knuckle-Boom Crane	27
4.1.1 Transformation Matrix from End-Eector to Base	28
4.1.2 Transformation of Joint Variable to Hydraulic Cylinder Position	30
4.1.3 Forward Kinematics	34
4.1.4 Inverse Kinematics by Using the Pseudoinverse Solution	36
4.1.4.1 Special Solution	36
4.1.4.2 Homogeneous Solution	36
4.1.4.3 Comprehensive Solution	36

..... 37	4.5 Gradient Projection Method	37	4.5.1
	Joint Limit Avoidance	37	4.5.2 Volumetric Flow
	Rate Reduction	39	4.5.3 Energy Optimization
..... 42	4.6 Inclusion of Hydraulic Transformer 46

v

Contents

	4.7 Integration of inverse solution in simulation model	47	
5	Evaluation 49	5.1 Results	49
	5.1.1 Test Trajectory	49	5.1.2 Simulation
Results	51	5.2 Discussion	58
6	Conclusion and Prospects 64	Bibliography 67	List of Figures 72
			List of Tables
			73
A	Appendix 74	A.1 Minutes of the Meeting	74
	A.2 Simulation Model	80	A.3 Source
	Code	81	A.4 Equations
	89	

Nomenclature

Acronyms

CTL cut-to-length
C-Space conguration space
DH Denavit Hartenberg
DOF degrees of freedom
FCR ow consumption rate
GPM gradient projection method
HT hydraulic transformer
IBC inner boom
JLA joint limit avoidance
OBC outer boom
T-Space task space
P-optimal power optimal
Q-optimal volumetric ow rate optimal
2D two dimensional
3D three dimensional
4D four dimensional

Latin Symbols

l m link length
 m m^2 performance criterion
 $\{x, y, z\}$ [-] coordinate system
 $\{x, y, z\}$ [-] coordinate system
 k [-] HT constant
 δ m link oset
 J J energy
 ρ [-] grapple of crane arm
 η [-] performance criterion
 $\Delta \eta$ [-] performance gradient

Nomenclature

I [-] unit matrix
 θ [-] joint of crane arm
 J [-] Jacobian matrix
 α [-] adjustment parameter

α_i [-], m link of crane arm, distance for mounting point \mathbf{p}_i m position in space

\bar{p} bar, $\frac{N}{m^2}$ pressure

P W power

θ_i m, ° joint position, cylinder position $\dot{\theta}_i$ $\frac{m}{s}$ joint velocity, cylinder velocity

\dot{V}_{min} $\frac{m^3}{s}$ volumetric flow rate

\mathbf{m}^2 dot product of unit vectors \mathbf{m} m vector between

two coordinate frames $\dot{\theta}_s$ operator input velocity

r-direction \hat{r} [-] cylindrical coordinate axis \mathbf{m}, s

translational vector, time \mathbf{m} transformation matrix

\mathbf{W} [-] weighting matrix

x_i m, [-] x-coordinate, joint coordinate axis

$\dot{\theta}_s$ operator input velocity \mathbf{p}_e m end-effector position

$\dot{\theta}_s$ $\frac{m}{s}$ end-effector velocity

\hat{x} [-] X-axis

y_i m, [-] y-coordinate, joint coordinate axis \hat{y} [-]

Y-axis

z_i m, [-] z-coordinate, joint coordinate axis

$\dot{\theta}_s$ operator input velocity z-direction \hat{z} [-]

cylindrical coordinate axis \hat{z} [-] Z-axis

{0} [-] coordinate system

{1} [-] coordinate system

{2} [-] coordinate system

{3} [-] coordinate system

{4} [-] coordinate system

Greek Symbols

α_i ° link twist

β_i [-] angle for transformation from joint to cylinder

γ_i [-] angle for transformation from joint to cylinder

δ_i [-] angle for transformation from joint to cylinder

ϵ_i [-] joint type

◊◊ ° joint angle, cylindrical coordinate axis

◊◊ ° operator slewing input

Indices

A coordinate system

B coordinate system, base frame

E end-effector coordinate system

h homogeneous solution

HT hydraulic transformer

i cylinder number

j joint number

JLA joint limit avoidance

LS load sensing

N total joint number

opt optimal algorithm

p piston side

P power optimal

Q volumetric flow rate optimal

r rod side

ref reference algorithm

s special solution

sys system

T matrix transpose

W weighting matrix

0 number of: coordinate system, link, joint

1 number of: coordinate system, link, joint

2 number of: coordinate system, link, joint

Nomenclature

3 number of: coordinate system, link, joint 4 number

of: coordinate system, link, joint + pseudoinverse

Jacobian matrix * adjusted pump flow

x

1 Introduction

1.1 Motivation

About one-third of Germany is covered by forest [7]. The demand for climate-neutral energy sources is growing in times of climate change and global warming. Furthermore, the amount of damaged timber rises due to insect infestations and droughts leading to an increase in timber felling. In 2019 the damage caused by insect infestations was responsible for half of the total 68 ·

10⁶ m³ felled timber in Germany. This requires intelligent measures to make the felling process more effective. At the same time, this process should be designed to be energy efficient. [38]

In the forestry industry, cut-to-length (CTL) logging has been established as the main felling process for large-scale production. In this process, the trees are cut by a harvester and limbed in the forest. The limbed stems are crosscut to the desired length by the harvester. A forwarder picks up these logs in the felling area and transports them to a roadside landing, where these are stored until pick up for long-distance transport. The loading and unloading process of the timber onto the load-space of the forwarder is accomplished by a knuckle-boom crane. This crane is maneuvered by an operator on the vehicle. Controlling this crane arm is a complex task for the operator. Until today in many forwarders, each joint of the crane arm is steered individually by the operator accordingly, to guide the crane tip through the workspace. Operators spend more than 70 % of their working time with crane manipulations [12]. Recent controls of knuckle-boom cranes simplify the task of controlling the crane arm for the operator, by solving the motion of each joint to the desired path computationally. This path is defined by the operator. Since the crane arm is a redundant system, an infinite number of configurations are given for each position. This redundancy can be used to advantage and optimized according to various performance criteria. Since fossil fuels are becoming increasingly scarce and emission savings are also an issue in forestry, an optimization with regard to the energy consumed by the crane motion is desirable. [30]

1.2 Scope of the Thesis

This thesis follows on from previous work. In a former thesis [24], an energy optimization solution is presented and included in a holistic simulation model. This approach searches for the minimum kinetic energy of the motion of a knuckle-boom crane. Furthermore, a hydraulic transformer, that uses potential energy due to contrary motions of the booms is included in this approach. Minimal kinetic energy does not necessarily lead to minimal energy consumption

f

o

r

1

1 Introduction

hydraulically actuated knuckle-boom cranes.

In a novel approach in this thesis, these circumstances shall be incorporated and

a minimal energy solution to the control of a knuckle-boom crane is searched. Therefore, local and global optimization algorithms should be compared and examined for the suitability of the given system. An appropriate algorithm should then be included in the existing simulation model. Furthermore, the hydraulic transformer is to be integrated into the system. The developed solution can then be tested regarding its efficiency.

1.3 Outline

The necessary fundamentals for understanding the approach of this thesis are explained in Chapter 2. For this purpose, commonalities in robotics are examined and kinematic principles are introduced. Furthermore, basic working principles of a load sensing system are conveyed. In Chapter 3 the structure of a forwarder and especially the knuckle-boom crane is presented. In regard to a minimal energy solution furthermore, a state of research on performance-optimizing algorithms is introduced.

Chapter 4 presents the implementation of the energy optimal algorithm for a given prototype. For this purpose, the gradient projection method is used. The performance gradient is a function of the current volume flow and cylinder pressure. The necessary steps are explained in detail and the formulas to derive this result are illustrated. Furthermore, the hydraulic transformer is included.

The results of a comprehensive test in a simulation model with regard to the effectiveness of the designed algorithm, are outlined in Chapter 5. Moreover, the validity of the working principle is discussed.

A conclusion of the thesis is given in Chapter 6

2 Fundamentals

This chapter presents the scientific fundamentals of a forestry crane. To describe the motion of a crane arm generically, basic kinematics of robotic manipulators are

introduced. Since forestry cranes are hydraulically actuated, the system characteristics of the working hydraulics are summarized.

2.1 Kinematics of Robotic Manipulators

The scientific study of the kinematics of knuckle-boom cranes, which are used on for warders is a relatively new eld of science. Due to the structure of the crane arm, similar problems of the kinematics can be found in industrial robotics, where this topic is inves tigated for a couple of decades. More precisely, the knuckle-boom crane of a forwarder can be compared to a serial link robot arm. In Figure 2.1 an industrial robot arm and a knuckle-boom crane on a forestry machine are presented. According to Siciliano [37], robotic mechanisms are systems of rigid bodies connected by joints. This classies the forwarder as a robotic mechanism. At the forwarder, the booms represent the rigid bodies that are connected by the joints. The grapple is considered the end-eector of the robotic arm.

The following sub-chapters describe the fundamentals of the methods used in this thesis, adapted from industrial robotics. To determine the motion of a serial link manipulator, basic robotic kinematics are introduced.

(a) Industrial robotic manipulator [2] (b) Knuckle-boom crane on forwarder [21]

Figure 2.1: Comparison of a industrial robotic arm and a forestry crane

2.1.1 Elementary Kinematics

The dynamics of a serial link manipulator can be divided into kinematics and kinetics. Kinematics describes the mechanical structure and motion of a body. Thereby masses of the body and forces, that are acting onto the structure, are not considered. Instead, these are investigated when looking at the kinetics of a system. The optimization method used in this thesis only focuses on the kinematics of a knuckle-boom crane. The system's kinetics are not taken into account. This simplies the complexity of the model in order to reduce computational eort. Furthermore, no information about the masses and their center of action is needed, which is variable for each payload and not always given. By applying the kinematics of a serial link manipulator, the location of a

$$\begin{aligned}
 & \hat{X}^t = \hat{Y} \hat{Z} \quad (2.2) \\
 & \hat{Y} = \begin{bmatrix} \hat{Y}_{11} & \hat{Y}_{12} & \hat{Y}_{13} \\ \hat{Y}_{21} & \hat{Y}_{22} & \hat{Y}_{23} \\ \hat{Y}_{31} & \hat{Y}_{32} & \hat{Y}_{33} \end{bmatrix} \quad (2.3) \\
 & \hat{X} = \begin{bmatrix} \hat{X}_1 \\ \hat{X}_2 \\ \hat{X}_3 \end{bmatrix} = \begin{bmatrix} \hat{Y}_{11} \hat{X}_1 + \hat{Y}_{12} \hat{X}_2 + \hat{Y}_{13} \hat{X}_3 \\ \hat{Y}_{21} \hat{X}_1 + \hat{Y}_{22} \hat{X}_2 + \hat{Y}_{23} \hat{X}_3 \\ \hat{Y}_{31} \hat{X}_1 + \hat{Y}_{32} \hat{X}_2 + \hat{Y}_{33} \hat{X}_3 \end{bmatrix} \quad (2.4) \\
 & \hat{X} = \begin{bmatrix} \hat{X}_1 \\ \hat{X}_2 \\ \hat{X}_3 \end{bmatrix} = \begin{bmatrix} \hat{X}_1 \\ \hat{X}_2 \\ \hat{X}_3 \end{bmatrix} \quad (2.5)
 \end{aligned}$$

Figure 2.3: Orientation, adapted from [11]

Pose The position and orientation of a rigid body are often expressed together and can be combined in one entity called pose. This combination is a set of four vectors. By looking at Figure 2.3 one vector (\hat{X}) denotes the position of point \hat{X} and three vectors explain the orientation (\hat{Y}). For example, frame $\{\hat{Y}\}$ is expressed in dependence of its position and orientation relative to $\{\hat{X}\}$: [11]

$$\{\hat{Y}\} = \{\hat{X}, \hat{Y}_{11}, \hat{Y}_{12}, \hat{Y}_{13}\} \quad (2.6)$$

To determine the displacement or motion of a rigid body in relation to an initial coordinate frame, its relative pose is dened via the relative transformation of two coordinate systems. One coordinate system refers to the rigid body, the second one is the initial frame. In respect thereof, the transformation matrix is used. This matrix consists of a rotational matrix and a translational vector for a three-dimensional coordinate frame, which are combined in a single 4x4 matrix.

Equation 2.8 describes this approach, where \hat{Y} represents the 3x3 rotational matrix and \hat{X} represents the translational 3D vector. \hat{X} and \hat{Y} represent a positioning vector in coordinate frame $\{\hat{X}\}$ and $\{\hat{Y}\}$, which describe the same point according to each coordinate system. [37, 10, 11]

$$\begin{aligned}
 & \hat{X} = \hat{Y} \hat{X} \quad (2.7) \\
 & \hat{X} = \begin{bmatrix} \hat{X}_1 \\ \hat{X}_2 \\ \hat{X}_3 \end{bmatrix} = \begin{bmatrix} \hat{Y}_{11} \hat{X}_1 + \hat{Y}_{12} \hat{X}_2 + \hat{Y}_{13} \hat{X}_3 \\ \hat{Y}_{21} \hat{X}_1 + \hat{Y}_{22} \hat{X}_2 + \hat{Y}_{23} \hat{X}_3 \\ \hat{Y}_{31} \hat{X}_1 + \hat{Y}_{32} \hat{X}_2 + \hat{Y}_{33} \hat{X}_3 \end{bmatrix} \\
 & \hat{X} = \begin{bmatrix} \hat{X}_1 \\ \hat{X}_2 \\ \hat{X}_3 \end{bmatrix} = \begin{bmatrix} \hat{X}_1 \\ \hat{X}_2 \\ \hat{X}_3 \end{bmatrix}
 \end{aligned}$$

2 Fundamentals

2.1.2 Task Space and Configuration Space

The previous kinematic formulations all refer to three-dimensional euclidean coordinate frames, which in robotics is named task space (T-space). Task space coordinates are user-orientated since the pose of the end-effector or each link can be expressed by main world coordinates. By looking at T-space coordinates, a pose of a body is directly pictured, whereas the pose of each link of a serial chain must be expressed separately or combined by using transformation matrices. Especially in an over-actuated system by expressing the end-effectors pose, the position of the links will not be dened. In contrast, the conguration space (C-space) is introduced. In conguration space, the pose of all joints can be expressed with the usage of only one coordinate point. The dimension of the C-space is dened by the number of joints of the observed serial link body. Each coordinate axis represents a single link of the system. The range of the coordinate axes is specied by the range of motion of the link. For revolute joints, an angular position is given, and for prismatic joints, the translational position along the joint axes is expressed. Hence, the system is fully dened by only knowing one coordinate point in C-space. [37, 10]

In Figure 2.4 the coordinate system representation of a serial link arm with two joints is shown. The task space coordinates are expressed by Equation 2.9. The detailed trans formation matrix is given in Equation 2.8. Since this example only has two joints, the transformation matrix gives the pose of frame $\{\diamond\diamond\}$. With more joints, the transformation matrix is a summary of all transformations and the explicit pose of each coordinate system can not be identified. For the same example, the C-space coordinates are given by 2.10. In this case, $\diamond\diamond_1$ and $\diamond\diamond_2$ describe rotational joints. A way of mapping the end-effector by knowing the C-space variables is presented in the following Chapter 2.1.4 and is known as forward kinematics.

By looking at the knuckle-boom crane as a serial link arm with four joints, it can be described in a 4D C-space.

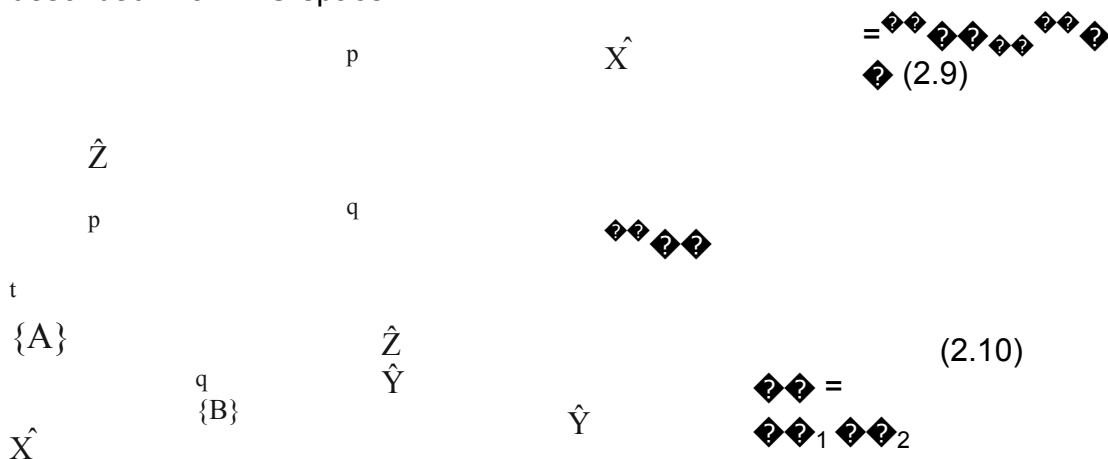


Figure 2.4: T-space and C-space

coordinates 6

2.1 Kinematics of Robotic Manipulators

2.1.3 Denavit-Hartenberg Parameters

Robotic arms are more formally named serial link manipulators. These can be defined as a chain of links that are connected by joints. The motion of each link affects the relative pose of each member of the chain. Aside from the base and the end-effector, the links in a serial chain manipulator are attached to one another through joints on both sides. With an increasing number of joints, the pose of the end-effector becomes a complex function of the state of each joint. [37, 10, 11]

Link A link is regarded as a rigid body that defines the spatial relationship of two neighboring joint axes of a serial chain manipulator. [11]

Joint Two neighboring links are connected by a joint. Each joint allows one degree of freedom and can either be rotational (revolute joint) or translational (prismatic joint). Figure 2.5 shows simple planar robotic arms. Example *a* presents a planar arm with one rotational degree of freedom $\diamond\diamond_1$, thus this joint is considered a revolute joint. In example *b* an additional revolute joint is added, hence by having two links this is the simplest configuration of a serial link manipulator. Similarly, example *c* consists of two links. $\diamond\diamond_1$ further on has a rotational degree of freedom, whereas $\diamond\diamond_2$ has a translational degree of freedom and reveals a prismatic joint. $\{0\}$ displays the base and $\{\diamond\diamond\}$ is the end-effector. [10]

Figure 2.5: Joint types of serial link manipulators [10]

"For a manipulator with $\diamond\diamond$ joints numbered from 1 to $\diamond\diamond$, there are $\diamond\diamond + 1$ links, numbered from 0 to $\diamond\diamond$. Joint $\diamond\diamond$ connects link $\diamond\diamond - 1$ to link $\diamond\diamond$ and moves them relative to each other. It follows that link $\diamond\diamond$ connects joint $\diamond\diamond$ to

joint $i+1$. Link 0 is the base of the robot, typically fixed and link n , the last link of the robot, carries the end-effector or tool" [10]. This convention limits the motion of each link and allows specific system simplifications. Denavit-Hartenberg introduced the notation named after him, which limits the system parameters due to constraints given by the system [22]. The notation uses only four instead of six parameters to describe the relationship between two coordinate frames while constraining the others. This limits the general applicability of this approach but simplifies the system if the application of Denavit-Hartenberg is permissible. The approach of only using four parameters is explained in Table 2.1 and is illustrated in Figure 2.6. [10, 11]

2 Fundamentals

Table 2.1: Denavit-Hartenberg Parameters [10]

Parameters	Variable	Description	Type of variable
Joint angle θ_i	θ_i	the angle between the Z_{i-1} and Z_i axes about the X_{i-1} axis	the X_{i-1} axis
Joint type	$\theta_i = 0$ for a revolute joint, $\theta_i = \infty$ for a prismatic joint		revolute joint variable prismatic joint
Link offset a_i	a_i	the distance from the origin of frame $i-1$ to the X_i axis along the Z_{i-1} axis	variable
Link length d_i	d_i	the distance between Z_{i-1} and Z_i axes along the X_i axis	constant
Link twist α_i	α_i	the angle from the Z_{i-1} axis to the Z_i axis about	constant

Figure 2.6: Denition of standard Denavit-Hartenberg link parameters

[10] 8

2.1 Kinematics of Robotic Manipulators

Due to the limitations made through applying the Denavit-Hartenberg method, the transformation matrix T_{i-1}^i from the coordinate frame located in joint $i-1$ to the coordinate frame located in joint i can be reduced to a standard Denavit-Hartenberg transformation matrix. This matrix only consists of elementary rotations and translations, as T_{i-1}^i , T_{i-1}^i , T_{i-1}^i and T_{i-1}^i . [10, 11]

$$T_{i-1}^i = T_{i-1}^i \circ T_{i-1}^i \circ T_{i-1}^i \circ T_{i-1}^i = T_{i-1}^i \circ T_{i-1}^i \circ T_{i-1}^i \circ T_{i-1}^i \quad (2.11)$$

$$T_{i-1}^i = \begin{bmatrix} \cos \theta_i & -\sin \theta_i & 0 & 0 \\ \sin \theta_i & \cos \theta_i & 0 & 0 \\ 0 & 0 & \cos d_i & -\sin d_i \\ 0 & 0 & \sin d_i & \cos d_i \end{bmatrix}$$

differential kinematics is applied for determining the end-effector's velocity. By differentiating Equation 2.15 with respect to time, Equation 2.16 is obtained. The task space velocity vector is given by \dot{p} , whereas q is the configuration space vector. [37, 10]

$$\dot{p} = \frac{d}{dt} f(q) = J(q) \cdot \dot{q} \quad (2.16)$$

$J(q)$ with respect to q is known as the Jacobian matrix. This matrix is a $n \times m$ matrix where n is the dimension of p and m is the dimension of q . The Jacobian matrix is built by the transposed gradient of each component of a vector. [37, 10]

$$J_{n \times m} = \begin{bmatrix} \frac{\partial f_1(q)}{\partial q_1} & \dots & \frac{\partial f_1(q)}{\partial q_m} \\ \vdots & \ddots & \vdots \\ \frac{\partial f_n(q)}{\partial q_1} & \dots & \frac{\partial f_n(q)}{\partial q_m} \end{bmatrix} \quad (2.17)$$

2.1.5 Inverse Kinematics

So far, only the forward kinematics are discussed. This means knowing the pose and rate of motion of each link, and thus being able to determine the end-effectors pose and rate of motion. Most problems in robotics are the inverse of this scenario. This means, determining the rate of motion of each joint, by knowing the pose of each link and having a desired end-effector velocity as a given input. The solution to this problem could be either found analytically (closed form) or numerically. This chapter describes a closed-form solution for solving the inverse problem. [37, 10]

Closed-Form and Numerical Solutions The inverse kinematics solution can either be determined by using a closed-form algorithm that implements geometric or algebraic approaches. The second option is finding an iterative numerical solution. With an increasing number of links, it becomes harder to find a closed-form solution. If the contemplated system is redundant, mostly several combinations of joint coordinates result in the same end-effector pose. Manipulators with a total of six degrees of freedom are solvable. Further restrictions must be made to find a closed-form solution. This can either be done by analytic expressions or by a polynomial solution of degree four or less in a way that non-iterative calculations suffice to find the solution. Numerical solutions include algorithms that optimize the inverse solution by multi-iterative methods according to a desired

analytic solutions and depending on the system. Thus, this approach is not real-time capable. [37, 10, 11]

By looking at the differential kinematics equation (Equation 2.18) for a square Jacobian matrix, which means $J = J^T$, the inverse solution is determined by regularly inverting the Jacobian matrix, where the inverse exists: [37, 10]

$$\dot{q} = J(q)^{-1} \cdot \dot{p} \quad (2.18)$$

For some end-effector poses in task space, an inverse solution does not exist ($J^{-1} = 0$). These joint configurations are called singularities and should be avoided. The task of solving the inverse solution becomes difficult when looking at redundant systems. A redundant system is defined by having more degrees of freedom than required to accomplish a requested task. This occurs if the robotic arm has more joints than degrees of freedom of the end-effectors motion. One approach to solve the inverse problem of a redundant system is the so-called Moore-Penrose pseudoinverse which was first introduced by Moore and simplified by Penrose and put into modern notation by Ben-Israel [5]. For a low rectangular and full-rank Jacobian matrix, its pseudoinverse can be expressed as follows. J^T expresses the transpose of the Jacobian matrix. Since only quadratic matrices ($J = J^T$) are invertible, the examined Jacobian matrix is multiplied by its transpose and then inverted. Thereafter, the inverted matrix is multiplied by the transpose again to generate the desired shape of rows and columns ($J^+ = J^T J^{-1}$ and $J^+ = J^T$). [37, 10]

$$J^+ = J^T (J J^T)^{-1} \quad (2.19)$$

The general solution is expressed in Equation 2.20. The velocities \dot{q} are the end-effectors velocity vectors in configuration space, and \dot{p}_0 is an arbitrary configuration space velocity vector. \dot{p} is the end-effector's velocity in the base frame coordinate system. The general inverse solution \dot{q} consists of \dot{q}_p , which is the special solution of the equation, and \dot{q}_h , known as the homogeneous solution. \dot{q}_p can be a stand-alone solution to the problem and provides the least square solution of the equation. This implies \dot{q} is solved to minimum joint velocity if $\dot{q}_h = 0$. By looking at the homogeneous solution, the term $(I - J^+ J)$ is the orthogonal projection matrix into nullspace of J , with I expressing the unit matrix. The homogeneous solution describes the self-motion of the serial link arm. Self-motion can only be seen in redundant systems and describes a motion of the links while the end effector remains in a constant position. The nullspace corresponds to the solution space of the inverse kinematics. Hence the homogeneous solution can be chosen accordingly to improve performance. [37, 10]

$$\dot{q} = \dot{q}_p + \dot{q}_h = J^+ \dot{p} + (I - J^+ J) \cdot \dot{p}_0 \quad (2.20)$$

2.1.6 Trajectories

The path of the end-effector between point A and point B over time is called a trajectory. For this purpose, two approaches can be used. Either Cartesian motion, which is a designated

2 Fundamentals

path in task space, or joint space motion, which is a designated path in configuration space. The pseudoinverse solution needs a given trajectory of the end-effector to solve the configuration of each joint per time step. Additionally, numerical solutions can propose a trajectory if only start and end point are given for the motion of a manipulator. This gives freedom for optimization for a path over time. Due to the capacity to choose the path, velocities, and accelerations accordingly to satisfy any performance criterion. [10]

2.2 Load Sensing Hydraulic Systems

To supply hydraulic energy to a multi-manipulator hydraulic system, mainly three different systems are used; Flow-controlled-systems, pressure-controlled systems, or complex controlled systems. These three systems can be distinguished by the way the hydraulic pump is controlled. The pump delivers the power needed to the hydraulic actuators. Load sensing systems are classified as complex-controlled systems. In classic load sensing systems, the pump displacement is controlled by the highest pressure of the system. The pressure applied to each manipulator is sensed and compared. The highest pressure required is forwarded to the pump controller and used to adjust the system pressure. The pump controller is designed to always exceed the load sensing pressure by Δp_{flow} . Due to system composition, only the volumetric flow rate needed is supplied by the pump.

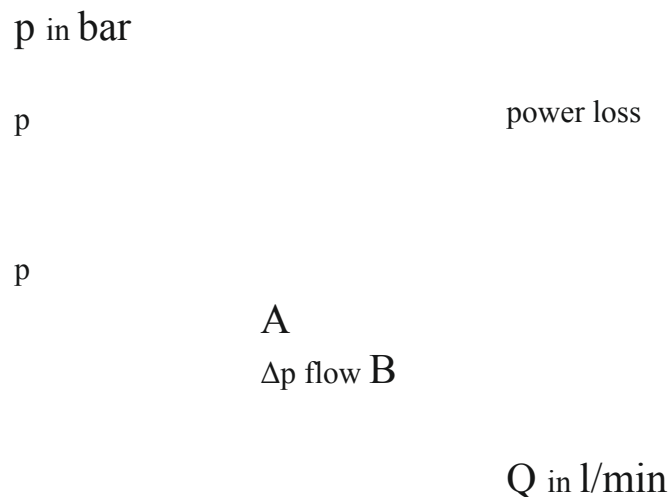


Figure 2.7: Performance of a load sensing system, adapted from [6]

$$P_{h, \text{total}} = \sum_{i=1}^n Q_i \cdot \Delta p_i \quad (2.21)$$

As it can be observed in Figure 2.7, the required hydraulic power is defined by the sum of the volumetric flow rate of all consumers and the difference of the overall load sensing

2.2 Load Sensing Hydraulic Systems

pressure to tank pressure. This correlation is shown in Equation 2.21. The difference of the system pressure and the pressure of each consumer multiplied by the corresponding flow rate are identified as power losses. As it can be seen in the diagram in Figure 2.7, the yellow area shows the power losses. This area becomes minimal for equal pressure of each consumer or for small volumetric flow rates of consumers with lower pressure. With a rising number of consumers, the power losses increase since for most working conditions the pressure of each consumer differs. By systematically reducing pressure peaks and additionally reducing the volumetric flow rate of each consumer, the power losses and thus the consumed power by the system can be reduced. [17, 18]

3 State of the Art

Firstly, the application range of forwarders and their structure and function are introduced. In a second sub-chapter, a state of the current research on optimizing energy consumption on knuckle-boom cranes is presented.

3.1 Technical Specifications of a Forwarder

In the following subsections, the structure and function of the forwarder is explained. Special attention is paid to the knuckle-boom crane.

3.1.1 Forwarder Design

"A forwarder is a log-loading and transport machine consisting of front and rear frames with six or eight wheels" [30]. Eight wheeled models often use bogies to increase traction as well as for soil-conserving maneuvering. The steering of a forwarder is implemented by an active articulated steering system. A passive rotational joint allows rotation between the front and rear frames of the vehicle. This ensures maximum traction while passing obstacles. The driver controls the machine from a cab, which is placed on the front frame. The rear frame consists of a load space on which the logs are loaded by a crane which is located on the front of the rear frame. The logs are secured by adjustable stakes. The hydraulic system consists of power train hydraulics, including hydraulic motors and steering cylinders, and working hydraulics to power the knuckle-boom crane. Both of which are powered by the internal combustion engine. A serial link hydraulic manipulator like the knuckle-boom crane is a mechanically complex rigid body structure. The crane consists of one rotational joint in the jaw direction and two joints in the pitch direction. Furthermore, a telescopic boom increases the reach of the knuckle-boom crane. At the end of the telescopic boom, a log gripper (grapple) is mounted and functions as an end-effector of the crane. This is visualized in Figure 3.1. Nowadays the working hydraulics are mostly managed by a load sensing system (Chapter 2.1.2), which regulates pressure and flow rate by hydro-mechanical feedback according to the power requirements. [30, 23]

14

3.1 Technical Specifications of a Forwarder

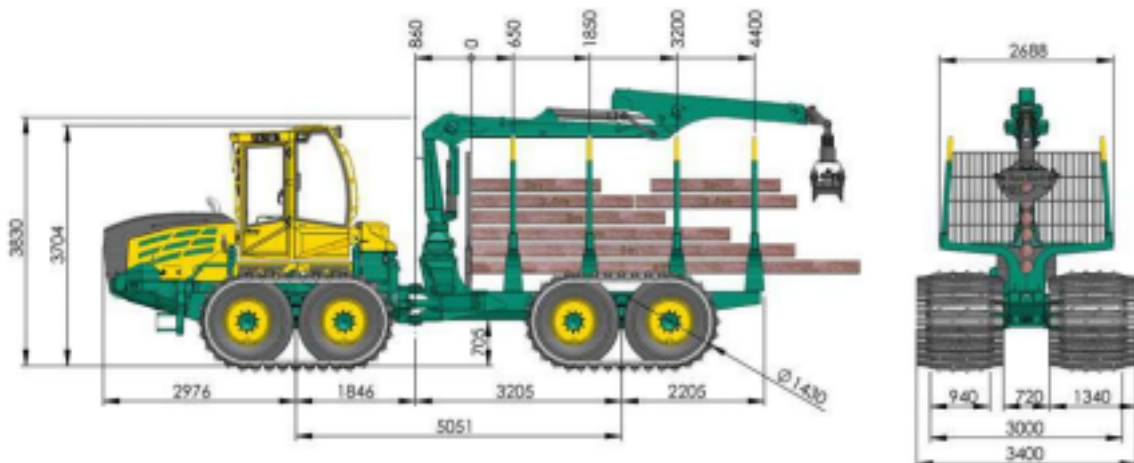


Figure 3.1: HSM BigFoot technical drawing [20]

3.1.2 Knuckle-Boom Crane

Figure 3.2 shows a 3D drawing of a knuckle-boom crane similar to the one discussed in this thesis. These cranes are designed to lift heavy payloads and are driven by hydraulic power. The knuckle-boom crane consists of four links and a grapple, which functions as an end-effector to grasp wooden logs. The links are connected by four joints and the grapple has additional links to ensure multiple degrees of freedom. The links are labeled as $L_1 - L_4$ similarly the joints are labeled as $J_1 - J_4$. Joints $J_1 - J_3$ have one rotational degree of freedom and J_4 has one translational degree of freedom. All joints are actuated by hydraulic cylinders.

Link L_1 is the base of the crane and functions as a mounting point, where the crane arm is mounted onto the vehicle base. J_1 also is the housing of the slewing mechanism J_1 , which allows an angular motion of the crane structure on a horizontal plane. In vehicle-based coordinates, this can be compared to a rotation around the yaw axis. J_1 connects the crane pillar L_2 with the crane base L_1 . The remaining joints $J_2 - J_4$ operate on a vertical plane. In combination with joint J_1 a 3D working space is generated. The inner boom L_3 is connected to the crane pillar by joint J_2 on one side. On the other side, the outer boom L_4 is attached through J_3 . The outer boom is hollow and houses the telescope joint J_4 . The grapple is mounted on the tip of the telescope unit.

J_2

L_2

$L_1 J_1$

J_3

$L_3 L_4$

J₄

G

Figure 3.2: Knuckle-boom crane, adapted from [25]

- ◆◆₁ Crane mounting bracket
- ◆◆₂ Crane pillar
- ◆◆₃ Inner boom
- ◆◆₄ Outer boom
- ◆◆ Grapple

3.2 Energy Optimization of the Knuckle-Boom Crane

As this thesis focuses on energy optimal solutions to control knuckle-boom cranes, this chapter presents hydraulic-mechanical methods to save energy during working cycles, as well as computational control algorithms to do so. In the first sub-chapter, a hydraulic transformer is presented. The second sub-chapter presents closed-form and numerical algorithms to control the crane arm.

3.2.1 Energy Savings Through a Hydraulic Transformer

During the loading process of a forwarder, the crane arm is raised and lowered to different heights to bypass obstacles or reach logs. This implies a difference in potential energy. Also on horizontal trajectories, due to the mechanical structure of the crane arm, the inner and outer boom execute a contrary motion, which leads to a difference of potential energy within two links. Whenever a boom is lowered while a second one is raised, the potential energy can directly be transferred between these two booms instead of dissipating as heat.

Therefore, the forwarder discussed in this thesis is equipped with a hydraulic transformer (HT). With this transformer, the hydraulic cylinder of the inner boom (IBC) and the hydraulic cylinder of the outer boom (OBC) are connected. This is shown by the hydraulic circuit in figure 3.3. A hydraulic transformer consists of two hydraulic pumps/motors, which can work both ways and function as both. These two displacement units are connected mechanically. Hence, the hydraulic power is transmitted mechanically from the OBC to IBC and vice versa. The two pump/motor units have the same displacement. Thus, the same volumetric flow rate adjusts on both sides of the hydraulic transformer.

The rod side of the OBC and the piston side of the IBC affect each other through the unit. If during a loading process, the inner boom $\diamond\diamond_3$ is lowered and the outer boom $\diamond\diamond_4$ is lifted, the potential energy from lowering the inner boom can be used to lift the outer boom. This mainly occurs during a lateral movement while reaching out to load or unload a log. The same process can be seen during a movement of the crane tip towards the machine, which occurs while loading logs onto the load space. The inner boom rises while the outer boom lowers. The potential energy of the outer boom is directly transferred into usable hydraulic energy to extend the IBC and thus raise the inner boom. According to Geiger et al. [16], the optimized hydraulic system with the hydraulic transformer saves energy up to 16 %. [16, 15]

F

LS

Figure 3.3: Hydraulic transformer, adapted from [15]

3 State of the Art

With an increase in electrification on mobile working machines, the regeneration of potential energy can alternatively be accomplished by electric generators and motors. Potential energy can thereby be stored using an onboard battery. This opens up the opportunity to use the potential energy independent of the current consumption. Hence, the energy could be transmitted beyond loading cycles and lead to greater efficiency. [1, 14, 27]

3.2.2 Presentation of Several Closed-Form and Numerical Solutions

Still today the task of controlling a knuckle-boom crane is done manually by a human operator. Over time, some simplifications have been developed to facilitate the work of the operator. Hereby, the main improvement was made by relieving the operator from manually solving the inverse kinematics of the crane arm, in order to maneuver the crane tip along the desired trajectory. Since in general, knuckle-boom cranes are redundant systems, this task copes with the difficulties entailed with redundancy. Whereas the redundancy also allows many possibilities to optimize the performance of the motion, which this chapter focuses on. For closed-form solutions, the task of planning the end effector's trajectory remains with the operator. The algorithms describing this task can be summarized as on-line instantaneous control solutions. In this thesis, on-line algorithms are limited to closed-form solutions. Due to low computational effort, these algorithms are real-time capable in most cases.

In a further step, the task of the operator can be simplified by also planning the trajectory through computational algorithms. The operators or intelligent assistance systems only determine the start and end position of the trajectory. Based on this given trajectory, a numerical algorithm can optimize the path of the manipulator as well as the speed of motion according to desired performance criteria. These algorithms are not real-time capable, due to heavy computational effort. Thus, the optimized trajectory must be computed in advance. Therefore, numerical solutions are classified as off-line solutions.

Furthermore, it is important to note, that on-line solutions of inverse problems only optimize the motion of a manipulator to a local optimum, since the trajectory can be continuously modified. Global solutions can only be derived using off-line algorithms, but their field of application is very limited to static conditions.

In the following two sub-chapters several on-line and off-line methods are presented, which solve the inverse problem appearing at the motion control of serial chain manipulators.

3.2.2.1 On-Line Control Solutions in Closed-Form

General information about closed-form solutions is provided in chapter 2.1.5. This chapter presents concrete proposals for the solution of the inverse problem considering the closed form. Furthermore, several performance optimization methods are presented. For most application cases on knuckle-boom cranes, these algorithms should deliver an on-line control solution, which means solving the desired control task in real-time.

Weighted Pseudoinverse Solution In 1969 Daniel Whitney introduced the control of a human arm prosthesis via pseudoinverse solution [41]. The inverse navigation significantly simplifies motion control of the prosthesis arm for the patient. Whitney implemented a cost function, thus the redundancy of the prostheses arm can be solved to superior performance. This cost function is embedded into the J^+ matrix (Equation 2.19) in a way that the special solution is solved to a minimum norm solution with respect to the cost function, which can be seen in the following

equations. Hereby, W is the cost function (weighting matrix) and u stands for the controller's input. \dot{q} describes the joint velocities: [41]

$$J_W^+ = W^{-1} \cdot J^+ \cdot (J \cdot W^{-1} \cdot J^+)^{-1} \quad (3.1)$$

$$\dot{q} = J_W^+ \cdot \ddot{p} \quad (3.2)$$

In 1999 Beiner and Mattila [3] adapted this approach and focused on the problem of optimizing the energy consumption of hydraulically actuated cranes. They extended this approach with the specificity of solving the pseudoinverse solution to minimal hydraulic actuator velocities instead of joint velocities while leaving the cost function as a unity matrix. This leads to low volumetric flow rates and pressure peaks can be avoided because of less acceleration. According to them, the locally minimized velocity results in an approximately minimized kinetic energy. As a second approach, the weighting matrix introduced by Whitney was modified in order to solve the inverse kinematics to minimal kinetic energy. Since the special solution \dot{q}_0 is a least-square solution of the joint velocity, it suggests itself to search for minimal kinetic energy. This is achieved by including the inertia matrix as the cost function. Thus, this term resolves to kinetic energy, which then is minimized by this function. According to the authors, this solution is fast and therefore most suitable for real-time control. Finally, the two approaches were compared and discussed. In the comparison of the two presented algorithms the former results in smoother and lower actuator velocities than the latter. Another disadvantage of the weighted pseudoinverse solution, presented by Beiner and Mattila, is the neglect of hydraulic energy losses caused by the fact, that all cylinders are driven by one pump and are controlled by a load-sensing system. The efficiency of this approach needs to be discussed since minimal kinetic energy of each link does not necessarily result in an energy optimal control according to the hydraulic system. [3]

Gradient Projection Method The gradient projection method (GPM) is a way of modifying the nullspace arbitrary vector \dot{q}_0 introduced in equation 2.20, in order to solve the redundancy of the pseudoinverse method according to the desired performance. In 1977 Alain Liègeois [26] proved, that it is possible to add any vector which is consistent with the constraints to the homogeneous solution as a performance vector. In this approach, the arbitrary nullspace vector of the homogeneous solution \dot{q}_0 was replaced by the gradient of a performance function Δ and multiplied by a real scalar vector α , which leads to the Equation 3.4. In order to minimize the performance function Δ , the constant α needs to be negative and vice versa to maximize Δ the constant α is taken as a positive scalar. A higher value of α achieves a faster optimization, whereas the maximum value of α is limited by the maximum joint velocities. By choosing the performance function wisely,

3 State of the Art

the performance of a redundant system can be optimized. In the following paragraphs, some examples are presented. [26, 19, 35]

$$\mathbf{q}_0 = \mathbf{q} \cdot \Delta \mathbf{q} \quad (3.3)$$

$$\mathbf{q} = \mathbf{J}^+ \cdot \mathbf{q}_0 + \mathbf{q} \cdot (\mathbf{I} - \mathbf{J}^+ \cdot \mathbf{J}) \cdot \Delta \mathbf{q} \quad (3.4)$$

Joint Limit Avoidance In many serial link manipulators, the joints' ranges of motion are restricted, due to mechanical boundaries. Avoiding these boundaries by solving the redundancy accordingly, can be done by using the weighted pseudoinverse solution or by gradient projection method. Both methods are presented. By using GPM the performance gradient $\Delta \mathbf{q}_0$ can be formulated as a position-dependent scalar performance criterion, which is minimized by projecting it onto the nullspace through the homogeneous solution of the pseudoinverse method. This performance criterion furthermore was used by Liègeois [26] to avoid joint limits. In order to accomplish this challenge, the performance criterion \mathbf{q}_0 is established to minimize the distance of the actual joint position \mathbf{q}_1 to the middle \mathbf{q}_m of the joint range. \mathbf{q}_{min} and \mathbf{q}_{max} represent the minimum and maximum joint positions. This correlation is given by Equation 3.5. The numerator of this equation becomes small by joint positions near the center of the link. Hence, the impact of this term on the performance gradient becomes low in these areas. The joint limit avoidance function (JLA) is individually determined for each joint and summed up subsequently. [26, 19]

$$= \sum_{i=1}^n \frac{1}{2} \left(\frac{\mathbf{q}_1 - \mathbf{q}_{min}}{\mathbf{q}_{max} - \mathbf{q}_{min}} \right)^2 + \frac{1}{2} \left(\frac{\mathbf{q}_1 - \mathbf{q}_{max}}{\mathbf{q}_{max} - \mathbf{q}_{min}} \right)^2$$

$$\mathbf{q}_0 = \mathbf{q}_1 - \mathbf{q}_m \quad (3.5)$$

The gradient vector $\Delta \mathbf{q}_0$ of the performance criterion \mathbf{q}_0 is generated by deriving \mathbf{q}_0 of each joint variable. The number of rows is given by the number of joints. [26, 19]

$$\Delta \mathbf{q}_0 = \frac{\partial \mathbf{q}_0}{\partial \mathbf{q}} = \frac{\partial}{\partial \mathbf{q}} \left(\frac{1}{2} \left(\frac{\mathbf{q}_1 - \mathbf{q}_{min}}{\mathbf{q}_{max} - \mathbf{q}_{min}} \right)^2 + \frac{1}{2} \left(\frac{\mathbf{q}_1 - \mathbf{q}_{max}}{\mathbf{q}_{max} - \mathbf{q}_{min}} \right)^2 \right) \quad (3.6)$$

Equation 3.5 was enhanced by Zghal [42] and put into Equation 3.7 by Chan and Dubey [8]. Both Equations 3.5 and 3.7 solve to minimum offset to the center of the joint range. In the secondly mentioned form, the gradient of the performance criterion is almost zero in the middle range and goes to infinity at either limit. The expression presented in Equation 3.7 is a standard practice to avoid joint limits. [8, 19, 34]

[9] presents a volumetric flow optimization of a redundant hydraulically actuated manipulator with seven joints. The main research goal is to avoid flow saturation in under-dimensioned hydraulic systems by reducing the volumetric flow rate demanded by the system. As a side effect, in a constant pressure system, savings of the overall energy consumption were observed. This approach uses a performance criterion to optimize the homogeneous solution of the pseudoinverse solution through GPM. The volumetric flow rate is a function of displaced volume over time. Hence, in a hydraulic cylinder the volumetric flow rate Q_{cyl} , as a function of the cylinder motion, is determined by multiplying the acting piston area A_{piston} by the corresponding cylinder velocity v_{cyl} . The acting cylinder area is distinguished in rod A_{rod} and piston A_{piston} side area depending on if the cylinder retracts or extends. [9]

$$Q_{cyl} = A_{piston} \cdot v_{cyl} \quad (3.10)$$

21

3 State of the Art

$$Q_{cyl} = \begin{cases} A_{rod} \cdot v_{cyl}, & \text{if } v_{cyl} \geq 0 \\ A_{piston} \cdot v_{cyl}, & \text{if } v_{cyl} < 0 \end{cases} \quad (3.11)$$

$$Q_{cyl} =$$

Cheng et al. stated, that depending on the structural integration of the hydraulic cylinder on a joint, the volume flow is a non-linear function of the joint velocity [9]. Furthermore, according to the size of the piston areas each joint demands a different volume flow. With having these challenges in mind, a performance criterion was defined, using the sum of all volume flows demanded, including leakage Q_{leak} . The Volume flows are functions of the joint angles, including their non-linear relations. The gradient of the performance criterion simplifies to the corresponding rod or piston area multiplied with the mentioned non-linear relation. [9]

$$\sum_{i=1}^n Q_{cyl_i} = A_{rod} \cdot v_{cyl_1} + A_{piston} \cdot v_{cyl_2} \dots \quad (3.12)$$

$$\Delta Q_{cyl} = \begin{cases} A_{rod} \cdot \Delta v_{cyl} \\ A_{piston} \cdot \Delta v_{cyl} \end{cases}$$

Furthermore by [9] it is proved, that a volumetric flow rate reduction can be combined with a joint limit avoidance criterion by adding the two performance gradients multiplied by the associated scalar λ . The combined expression is described in Equation 3.13: [9]

$$\Delta Q_{cyl} = J^+ \cdot \Delta v_{cyl} + (1 - J^+ \cdot J) \cdot (\lambda \cdot A_{rod} \cdot \Delta v_{cyl} + \lambda \cdot A_{piston} \cdot \Delta v_{cyl}) \quad (3.13)$$

Obstacle Avoidance Through Artificial Potential Fields Wang et al. [40] introduce a trajectory planning algorithm for redundant manipulators, with the target to avoid obstacles. For this purpose, the obstacles are bounded by assigning a repulsive potential field to them. With greater distance from the obstacle the repulsive fields abate. Furthermore, the start position also has a repulsive potential, whereas an attractive potential field is assigned to the end position. In consideration of each joint, a collision-free path is computed by following the areas of attractive potential and avoiding the areas of repulsive potential.

In the same manner, Luo et al. [29] applies collision-free path planning for a six-DOF serial harvesting robot in an energy optimal way. The potential field approach is used to avoid collision with obstacles in the use of axis-aligned bounding boxes in joint space. These bounding boxes are used to assign a repulsive potential to the obstacles. The possible collision-free trajectories are then optimized in search of minimum energy. This is achieved by a minimum sum of weighted rotating joint angles in joint space. The possible trajectories are optimized analytically towards the minimum sum of joint rotations in use of Matlab. This leads to an optimization of minimum energy, because it is assumed that all joints are energetically similar. [40, 29]

3 State of the Art

3.2.2.2 O-Line Control Solutions

This chapter presents three global solutions of either predefined trajectories or point-to-point solutions, which do not require a predefined trajectory. Since global solutions are not real-time capable, these are classified as o-line solutions. Some of these solutions could prove real-time capability under high computational effort. In respect thereof, a trajectory must be predicted at each time step, for the operator's input [32]. Due to the spontaneity of the operator, this approach would not inevitably deliver a global solution of the driven trajectory. With increasing autonomy, o-line solutions gain in importance. Especially on forwarders, loading cycles resemble ordinary loading cycles. Hence, a small number of trajectories could cover the active part of the working space [33]. These trajectories can be optimized to any performance criterion in advance.

Global Optimization Through Dynamic Programming The dynamic programming approach is a powerful, discrete-time algorithm that can provide a global solution to an optimization problem. For this purpose, performance criteria must be defined in form of a cost function. This cost function then is optimized over a given trajectory to a global minimum solution. The continuous-time problem needs to be divided into smaller discrete time steps, in which the problem can be solved by a numerical algorithm. By choosing the time steps sufficiently small, the approximation to the global solution becomes greater, but the computational time rises. In search of a global solution, these time-frames are not independent of each other. Thus, the discrete-time problems share common sub-problems. An algorithm that solves these sub-problems to a minimum predefined cost was introduced by Richard Bellman [4]. This algorithm stores the optimal solutions of the increments to avoid computing them several times and then compares them for the best solution. In search of a global optimum of the defined performance

criterion, this solution is found in two phases. In a first phase, the given path is analyzed backwards for the lowest possible input variables. In a second phase, the position, velocity, and acceleration of each joint are searched to a minimal cost for the given input variables. This second phase proceeds from the start to the endpoint of the trajectory.

The complexity of the problem rises with increasing degrees of freedom. Hence, dynamic programming can only be applied to practical approaches when the number of dimensions is low. In practice, this can be achieved by only optimizing one joint and solving the others by inverse kinematics. This approach limits the redundancy and leads to less complex numerical solutions. [28, 4, 32, 31]

Löfgren [28] introduced a global optimization to minimize trajectory times for a manipulator, to maneuver from a start point to an endpoint in an obstacle-free workspace. For this purpose, a dynamic programming algorithm in the manner of Bellman is used to generate the optimal path. Due to heavy computational effort, this method can be used to optimize predefined working cycles to time efficiency.

Nurmi and Matilla [32, 31] found a global energy solution through the dynamic programming approach for a hydraulically actuated manipulator. The suitability of the proposed algorithm for constant pressure and load sensing systems is examined. The redundancy of the manipulator is solved by pseudoinverse solution in respect of the hydraulic actuator coordinates. Furthermore, the system dynamics are considered by using the Euler method.

24

3.2 Energy Optimization of the Knuckle-Boom Crane

Under consideration of the system's dynamics, a cost function is formulated including the volumetric flow rate with respect to the system's kinetics, as well as the pressure of the hydraulic system. To reduce the complexity of the solution the optimization of the redundancy of the system is limited to the telescope joint. The remaining joints are solved through inverse kinematics. In comparison to local optimization, the global solution achieves a 15-30% smaller energy consumption. However, this algorithm can only be utilized for predefined trajectories since this off-line solution is not real-time capable. Predicted solutions could be used to apply this algorithm on on-line applications, but only to a limited degree of complexity. [32, 31]

Global Energetic Solution Through Lagrangian Energy Function Saramago and Steen JR. [36] present a global solution through Euler-Lagrange's equation in the use of Lagrange's energy function, to minimize the kinetic and potential energy of a trajectory. This equation is resolved into three components: The Coriolis forces, the centripetal forces, and the gravity loading vector. Hence, the equation is a function of the joint velocity and acceleration as well as the geometric relations expressed in the transformation matrix of the manipulator and the masses including their center of action. In a second performance criterion, the trajectory is optimized to minimum executive time. Both criteria are considered in an off-line solution through a numerical approach. To find the pseudo-objective function in respect of the Lagrangian performance criterion, polynomial functions of local optimization are splined together. This leads to an optimized trajectory formulated in the use of spline functions. [36]

4 Methods

This chapter focuses on the methods used, to realize energy optimization on a forwarders knuckle-boom crane. The forwarder discussed in this thesis is a HSM 208F forestry machine. The knuckle-boom crane is manufactured by Palinger Epsilon, model S100F 101.

Determination of the Method to Be Used The aim of reducing the energy consumption induced by the motion of the crane arm is implemented by use of the pseudoinverse solution in combination with the gradient projection method (Chapter 3.2.2.2). This approach consigns the operator to individual control of the desired path. Hence, the energy consumption is optimized in the whole workspace and even unusual loading processes can be optimized towards minimal energy consumption. The produced algorithm is classified as an on-line solution in closed form. Thus, the approach searches for a local optimum in each time step. With this method, the trajectory is not optimized globally. A local optimization was explicitly chosen because the computing capacities on the machine are limited. Real-time optimization is important to ensure the exibility of the loading cycles and thus to guarantee a reduction of the energy in exceptional situations. No predesigned trajectories are needed since the operator's input is directly permuted into an energy-sparing motion of the system. To avoid singularities a joint limit avoidance is added to the performance criterion. The energetic reducing algorithm is established by adapting the approach, of minimizing the volumetric ow rate presented by Cheng et al. [9], to the introduced machine. This approach seems most suitable to optimize the energy consumption on a hydraulic level since in [9] the energy consumption of a constant pressure

system was minimized successfully. The algorithm is extended and adapted to the load sensing system in order to reduce the system pressure. To the author's knowledge, this method is unique compared to the other energy optimization methods, as no knowledge of the system dynamics is necessary to minimize the hydraulic energy. This simplifies the model and reduces computational effort. Furthermore, the algorithm is designed suitable for any load weight, as direct feedback is always provided by the system. This is not necessarily guaranteed for methods with fixed dynamic correlations.

In the following sub-chapters, the exact procedure for the development of this algorithm is presented as follows: Firstly, the kinematics of the discussed crane arm is defined by applying Denavit Hartenberg notation. Furthermore, the joint coordinates are transformed to actuator coordinates of hydraulic cylinders. These partly non-linear transformations allow optimization on a hydraulic level. Using the transformation matrices, the inverse kinematics for controlling the crane tip is set up directly as a function of the actuator coordinates. A performance gradient is established through the gradient projection method. This gradient consists of a joint limit avoidance method as well as an energy minimization

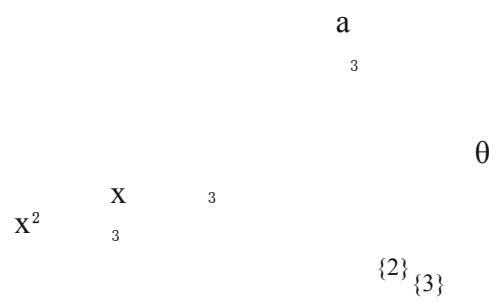
26

4.1 Denavit Hartenberg Notation of the Knuckle-Boom Crane

approach. In respect thereof, a volume flow minimization is established as a gradient of the total volume flow of the system. This gradient is supplemented with the actual cylinder pressure. By raising the pressure to a higher power, the influence of the pressure on the efficiency of the algorithm is increased. The implementation of this algorithm is embedded in an existing simulation model of the crane arm in the simulation software Simulink Matlab.

4.1 Denavit Hartenberg Notation of the Knuckle-Boom Crane

By applying Denavit Hartenberg notation, as explained in Chapter 2.1.3, the pose of each joint and link can be described by only using four parameters per joint and corresponding link. As it can be observed in Figure 4.1, five coordinate systems are necessary to fully describe the motion of the crane arm. The main coordinate system ($\{0\}$, $\{1\}$, $\{2\}$) is located in the base of the crane arm $\{0\}$ and is a spatially fixed cylindrical coordinate system. The motion of the crane tip along these three main coordinate axes is directly controlled via a joystick by the operator. The operator controls the motion of coordinate frame $\{4\}$, where the end-effector is located relative to the base frame $\{0\}$.



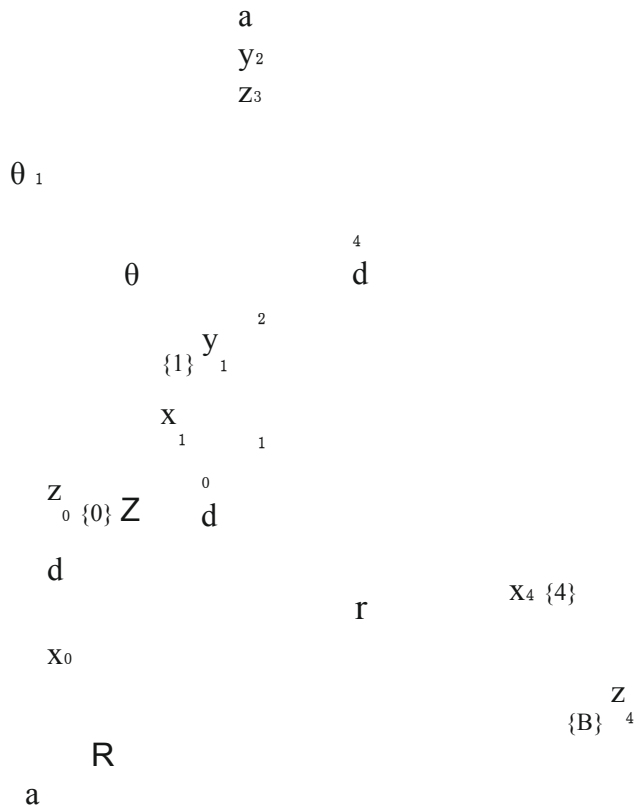


Figure 4.1: Denavit Hartenberg notation on knuckle-boom crane, adapted from

[2

4]

2

7

4 Methods

Coordinate system $\{0\}$ is located in the center of the slewing joint $\diamond\diamond_1$ (joint numbers are assigned in chapter 3.1.2). In the center of joint $\diamond\diamond_2$, coordinate frame $\{1\}$ is located. Similarly, coordinate system $\{2\}$ is located in the center of joint $\diamond\diamond_3$. Since joint $\diamond\diamond_4$ is a prismatic joint, it needs two coordinate frames to fully describe its motion, which is the distance between coordinate frame $\{3\}$ and $\{4\}$. Frame $\{4\}$ is located in the mounting point of the grapple. Frame $\{3\}$ is located on an imaginary line, parallel to the telescope joint and fully dened through crossing the mounting point of the end-eector. Frame $\{3\}$ is located where this imaginary line and a second imaginary line, which is normal to the rst one, cross. The second imaginary line is fully dened by the intersecting point in the

center of joint $\{3\}$.

4.1.1 Transformation Matrix from End-Eector to Base

To generate the overall transformation matrix from the end-eectors coordinate system to the base frame, the transformation matrices from each coordinate frame to the following must be determined and henceforth multiplied. This is done by nding the Denavit Hartenberg parameters and lling these into the Denavit Hartenberg transformation matrix (Equation 2.12) as explained in Chapter 2.1.3.

Table 4.1: Denavit-Hartenberg parameters of the knuckle-boom crane

Number of Joint	θ_j	d_j	a_j	α_j
0	0	0	a_0	0
1	θ_1	d_1	a_1	$-\alpha_2$
2	θ_2	0	a_2	0
3	θ_3	0	a_3	$-\alpha_2$
4	0	0	a_4	0

The frames $\{0\}$ and $\{a_0\}$ are displaced by distance a_0 but have the same orientation. Hence, no rotation is needed and the only translation is observed in a_0 direction. Equation 4.1 expresses the mentioned transformation in a 4 x 4 matrix.

$${}^0T_{a_0} = \begin{bmatrix} 1 & 0 & 0 & a_0 \\ 0 & 1 & 0 & 0 \\ 0 & 0 & 1 & 0 \\ 0 & 0 & 0 & 1 \end{bmatrix} \quad (4.1)$$

The motion of joint θ_1 results in a rotation between coordinate systems $\{0\}$ and $\{1\}$. θ_1 describes the angle between the two frames, as can be seen in the orientation matrix of ${}^0T_{\theta_1}$. Furthermore, the two coordinate systems are rotated about the θ_1 -axis by an angle of

4.1 Denavit Hartenberg Notation of the Knuckle-Boom Crane

$\theta_1 = -\alpha_2$. Since θ_1 is constant, the numerical value is already substituted in Equation 4.2, and sinus and cousins simplify to -1 and 0. Additionally frames $\{0\}$ and $\{1\}$ are translated along the θ_1 -axis by distance a_1 and along the a_0 -axis by a_1 . Due to the mentioned rotations, the two translations result in a three-dimensional translation.

$${}^0T_{\theta_1} = \begin{bmatrix} \cos \theta_1 & \sin \theta_1 & 0 & a_1 \\ \sin \theta_1 & \cos \theta_1 & 0 & a_1 \\ 0 & 0 & 1 & 0 \\ 0 & 0 & 0 & 1 \end{bmatrix}$$

$${}^1_2 T_2 = \begin{bmatrix} \cos \theta_2 & -\sin \theta_2 & 0 & 0 \\ \sin \theta_2 & \cos \theta_2 & 0 & 0 \\ 0 & 0 & 1 & 0 \\ 0 & 0 & 0 & 1 \end{bmatrix} \quad (4.2)$$

Coordinate system {1} and {2} have an equal orientation of the \hat{x}_1 -axis, but the \hat{x}_2 - and \hat{z}_2 -axes are rotated by the angle θ_2 , which describes the motion of joint θ_2 . The two frames are displaced by distance a_2 along the \hat{x}_2 -axis. The transformation of these two frames is summarized in the transformation matrix ${}^1_2 T_2$, which is assigned as Equation 4.3.

$${}^1_2 T_2 = \begin{bmatrix} \cos \theta_2 & -\sin \theta_2 & 0 & a_2 \sin \theta_2 \\ \sin \theta_2 & \cos \theta_2 & 0 & a_2 \cos \theta_2 \\ 0 & 0 & 1 & 0 \\ 0 & 0 & 0 & 1 \end{bmatrix} \quad (4.3)$$

Similar to joint θ_2 , also θ_3 is rotated along the \hat{x}_2 -axis. The angle of rotation is expressed as angle θ_3 . In the same manner, coordinate systems {2} and {3} are not rotated along other axes and are translated by distance a_3 along the \hat{x}_3 -axis. The resulting transformation is expressed in Equation 4.4. Due to Denavit Hartenberg notation for a rotational angle of $\theta_2 = 0$, both joints θ_2 and θ_3 result in an angle of θ_2 between the previous and the following link. A clockwise rotation of these two joints results in a positive θ_2 angle.

$${}^2_3 T_3 = \begin{bmatrix} \cos \theta_3 & -\sin \theta_3 & 0 & a_3 \sin \theta_3 \\ \sin \theta_3 & \cos \theta_3 & 0 & a_3 \cos \theta_3 \\ 0 & 0 & 1 & 0 \\ 0 & 0 & 0 & 1 \end{bmatrix} \quad (4.4)$$

The translation joint θ_4 is dened by the variable distance a_4 . No rotation or other translations are applied. This reduces the transformation matrix to a unit matrix with a transla

4 Methods

$${}^4_4 T_4 = \begin{bmatrix} 1 & 0 & 0 & 0 \\ 0 & 1 & 0 & 0 \\ 0 & 0 & 1 & 0 \\ 0 & 0 & 0 & 1 \end{bmatrix} \quad (4.5)$$

tional variable in \hat{x}_4 direction (Equation (4.5))

$${}^4_4 T_4 = \begin{bmatrix} 1 & 0 & 0 & 0 \\ 0 & 1 & 0 & 0 \\ 0 & 0 & 1 & 0 \\ 0 & 0 & 0 & 1 \end{bmatrix}$$

The overall transformation matrix from frame {4} to the base frame $\{0\}$ is

computed by the multiplication of all single transformation matrices, as presented in Equation 4.1.1. Only the angles $\theta_1, \theta_2, \theta_3$ and the distance d_4 are variable and constitute the joint variables. The remaining lengths are constants and are specific dimensions of the investigated knuckle-boom crane.

$${}^0T_4 = {}^0T_0 {}^0T_1 {}^1T_2 {}^2T_3 {}^3T_4 = (4.6)$$

$$\begin{bmatrix} \cos(\theta_2 + \theta_3) \cos \theta_1 & \sin \theta_1 & 0 & 0 \\ \cos(\theta_2 + \theta_3) \sin \theta_1 & -\sin \theta_1 & 0 & 0 \\ 0 & 0 & \cos \theta_1 & 0 \\ 0 & 0 & 0 & 1 \end{bmatrix}$$

(
 θ_1
 θ_2
1
+
 θ_3
 θ_4
3
c
o
s
(
 θ_1
 θ_2
2
+
 θ_3
 θ_4
3
)
-
 θ_1
 θ_2
4
s
i
n
(
 θ_1
 θ_2

4.2 Transformation of Joint Variable to Hydraulic Cylinder Position

The joints on knuckle-boom cranes are actuated hydraulically to provide large forces. Therefore, hydraulic cylinders supply the needed momentum to perform the required motion while lifting heavy payloads. These hydraulic cylinders are mounted on both links of a mechanical joint. The distance between the joint and the mounting point of the hydraulic cylinder generates a lever arm to apply momentum. The momentum varies depending on the angle of the impressed force. Hence, the motion of the joint is a function of the hydraulic cylinder motion. This implies, that also the joint location is a function of the actual cylinder length. For the rotational joints θ_2 and θ_3 , these functions are nonlinear and are only solvable for certain angular ranges. Through the limited stroke of the hydraulic cylinders, the avoidance of these non-solvable ranges, also called singularities is mechanically implemented. The computational avoidance of these ranges is presented in a following chapter. Joint θ_4 is a prismatic joint, which means that the transformation to the hydraulic cylinder coordinates is a linear function. The following sub-chapters describe the correlations between the actual cylinder lengths (indicated as l_1 , l_2 , l_3) and the joint variables θ_2 , θ_3 , θ_4 . θ_1 is not mentioned due to system simplifications explained in Chapter 4.3.

30

4.2 Transformation of Joint Variable to Hydraulic Cylinder Position

Transformation of θ_2 to Cylinder Position l_1

Joint θ_2 is actuated by a hydraulic prismatic cylinder and the total length of the cylinder is given by the variable l_1 . Figure 4.2 shows the kinematic correlation between l_1 and θ_2 . The joint angle θ_2 can be computed, by summing the angles θ_{11} , θ_{12} , θ_1 :

$$\theta_2(l_1) = \theta_{11} + \theta_{12} + \theta_1(l_1) \quad (4.7)$$

The angles θ_{11} and θ_{12} are fixed angles. θ_{11} is spanned between lengths l_{11} and the vertical axis introduced in the previous chapter as l_1 . θ_{12} is spanned between l_{12} and the inner boom (Figure 4.2). l_{11} and l_{12} are the distances from θ_2 to the two anchor points of the hydraulic cylinder. The angle θ_1 is spanned between l_{11} and l_{12} and therefore directly depends on the current length of the hydraulic cylinder l_1 . To compute θ_1 the law of cosines is applied as can be seen in Equation 4.8. By substituting Equation 4.7 and Equation 4.8 θ_2 can be expressed as a function

of θ_1 .

$$\theta_1(\theta_1) = \arccos \frac{L^2 + l_1^2 - l_2^2}{2 \cdot L \cdot l_1} \quad (4.8)$$

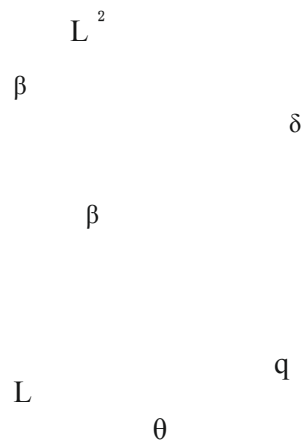


Figure 4.2: Kinematics transformation of θ_2 to θ_1 , adapted from

[

2

4

]

3

1

Transformation of α_3 to Cylinder Position α_2

The expression of α_3 as a function of α_2 is more complex because of two deflection levers (α_{221} and α_{222}) between the anchor point of the hydraulic cylinder and the inner and outer boom (Figure 4.3). α_{222} is a deflection length and directly dependent on length α_2 , which is the actual length of the hydraulic cylinder. To solve the trigonometric problem of the transformation, the structure can be divided into two main parts: The lever connected onto the inner boom and the lever connected onto the outer boom. By looking at Figure 4.3, this means left and right side of length α_{222} . To solve the transformation, firstly the angle α_{222} is determined by using the law of cosines. This angle is spanned between lever arm α_{221} and length α_{225} (anchor point of hydraulic cylinder to lever arm bearing point) around the bearing point of the lever arm. α_{222} is a function of α_2 (Equation 4.9).

$$\alpha_{222}(\alpha_2) = \arccos \frac{\alpha_{225}^2 + \alpha_{221}^2 - \alpha_2^2}{2 \cdot \alpha_{225} \cdot \alpha_{221}} \quad (4.9)$$

$\alpha_{21}(\alpha_2)$ is determined by subtracting $\alpha_{222}(\alpha_2)$ from constant angle α_2 .

$$\alpha_{21}(\alpha_2) = \alpha_2 - \alpha_{222}(\alpha_2) \quad (4.10)$$

The length of the deflection lever arm α_{222} , as a function of α_2 , is determined using the law of cosines. α_{224} is a constant distance between the bearing point of the left lever arm and joint α_3 .

$$\alpha_{222}(\alpha_2) = \sqrt{\alpha_{224}^2 + \alpha_{221}^2 - 2 \cdot \alpha_{224} \cdot \alpha_{221} \cdot \cos(\alpha_{21}(\alpha_2))} \quad (4.11)$$

To calculate $\alpha_{21}(\alpha_2)$, which is the angle between α_{222} and α_{224} around joint α_3 , the law of sinus is applied. The sum of all angles in a triangle is π . By subtracting α_{21} and the remaining angle, determined by the law of sinus, from π , the angle $\alpha_{21}(\alpha_2)$ is calculated.

$$(\alpha_2)$$

$$\alpha_{21}(\alpha_2) = \pi - \alpha_{21} - \arcsin \frac{\alpha_{224}}{\alpha_{222}(\alpha_2) \cdot \sin(\alpha_{21})} \quad (4.12)$$

$$\arcsin \frac{\alpha_{224}}{\alpha_{222}(\alpha_2) \cdot \sin(\alpha_{21})}$$

$$\alpha_{222}(\alpha_2) \cdot \sin(\alpha_{21})$$

To solve the remaining unknown angles, the lever arm connected to the outer boom is observed. $\alpha_{222}(\alpha_2)$ is computed by the law of cosines, by substituting α_2 . This leads to Equation 4.13, where α_{222} is the length of

the lever arm connected to the outer boom and L_{223} is the distance from the bearing point of the lever arm L_{222} to joint O_3 . α_{22} (α_2) is spanned between these two lengths.

$$\alpha_{23}(\alpha_2) = \arccos \frac{L_{222}^2 + L_{223}^2 - L_{22}(\alpha_2)^2}{2 \cdot L_{222} \cdot L_{223}} \quad (4.13)$$

32

4.2 Transformation of Joint Variable to Hydraulic Cylinder Position

α_{22} (α_2) is calculated similarly to the left side by using the law of sines.

$$\alpha_{22}(\alpha_2) = \alpha_2 - \alpha_{23} - \arcsin \frac{L_{223} \sin(\alpha_{23}(\alpha_2))}{L_{22}(\alpha_2)} \quad (4.14)$$

Finally α_3 (α_2) is computed by summing up the angles α_{21} (α_2), α_{21} , α_{21} (α_2) and α_{21} . Thereby, α_{21} is the angle between L_{224} and the inner boom and α_{22} is the angle between L_{223} and the O_3 -axis of frame {3}.

$$\alpha_3(\alpha_2) = \alpha_{21}(\alpha_2) - \alpha_{21} + \alpha_{22}(\alpha_2) + \alpha_{22} - \alpha_2 \quad (4.15)$$

$$L_{221}^2 L_{122}^2$$

$$\gamma_{23} \delta^2 L$$

$$\frac{\gamma}{L_{22}^2} \theta^2 \frac{L_{222}}{L_{22}} \frac{L_{225}}{L_{22}^2} \beta^2$$

Figure 4.3: Kinematics transformation of d_{32} to d_{21} , adapted from [24]

Transformation of d_{43} to Cylinder Position d_{32}

The position of the telescope cylinder and thus the total length of the outer boom d_{43} is linearly dependent on the hydraulic cylinder position inside the telescope arm. The variable extension of the telescope arm consists of two segments. The first one is guided linearly in the inner boom, the second segment is guided similarly in the first segment. These two segments are connected through a chain, therefore the actual telescope position is twice the hydraulic cylinder position. The total length of the outer boom is computed by adding the minimal length d_{32} .

$$d_{43}(d_{32}) = d_{32} + 2 \cdot d_{32} \quad (4.16)$$

d_4

$$L_3^{q_{3 \times 2}}$$

Figure 4.4: Kinematics transformation of d_{43} to d_{32} , adapted from [24]

4.3 Forward Kinematics

The basic mathematics of the forward kinematics are introduced in the fundamentals (Chapter 2.1.4). The forward kinematics of the knuckle-boom crane

are described according to therein dened notations. For this purpose, the vector \mathbf{p}_{04} is introduced, which is a vector from the center of the base coordinate frame $\{0\}$ to the center of the coordinate frame $\{4\}$, which is assigned as the end-ector of the system (Figure 4.1). To generate this vector, the overall transformation matrix \mathbf{T}_{04} is multiplied by the zero point of coordinate frame $\{4\}$ in Equation 4.17. The fourth dimension of this vector is necessary due to the general form of the transformation matrix. This multiplication simplifies the transformation matrix to the translational vector. This vector is located in the last column of the matrix.

$$\mathbf{p}_{04} = \mathbf{T}_{04} \begin{bmatrix} 0 \\ 0 \\ 0 \\ 1 \end{bmatrix} = \begin{bmatrix} \cos \theta_1 (a_1 + a_2 \cos \theta_2) + a_3 \cos(\theta_2 + \theta_3) \\ \sin \theta_1 (a_1 + a_2 \cos \theta_2) + a_3 \sin(\theta_2 + \theta_3) \\ a_2 \sin \theta_2 \\ 0 \end{bmatrix} \quad (4.17)$$

Due to specivities of the knuckle-boom crane's structure, joint θ_1 is the only joint solely operating in the horizontal plane of the base coordinate system, thus the rotation around the θ_1 -axis is independent of the remaining joints. Hence, the transformation of the base frame to a cylindrical coordinate system is considered. This transformation is expressed in Equation 4.18. The cylindrical base coordinate frame consists of the two axes, θ_1 , θ_2 , and an angle Θ , which describes a rotation around the θ_1 -axis. The orientation of the base coordinate frame does not change, but the θ_2 -axis is replaced by the θ_3 -axis. The independence of joint θ_1 is proved by comparing vector \mathbf{p}_{04} of the spatial coordinate frame

with the vector $\mathbf{p}_{4,\Theta}$ of the cylindrical coordinate frame. In vector $\mathbf{p}_{4,\Theta}$ the joint variable θ_1 only appears in the Θ component. The Θ component solely is described by the joint angle θ_1 . The θ_2 and θ_3 components of the vector are independent of θ_1 . This circumstance enables simplifying the forward kinematics and all following considerations to a two-dimensional problem in a vertical plane spanned by the θ_2 - and θ_3 -axes.

$$\mathbf{p}_{04} = \begin{bmatrix} \cos \theta_1 \mathbf{p}_{4,\Theta} \\ \sin \theta_1 \mathbf{p}_{4,\Theta} \\ 0 \\ 0 \end{bmatrix} = \begin{bmatrix} \cos \theta_1 \sqrt{a_2^2 + a_3^2} \\ \sin \theta_1 \sqrt{a_2^2 + a_3^2} \\ a_2 \\ 0 \end{bmatrix}$$

can be optimized towards a desired performance. This opens the door for optimization of the crane motion in every aspect.

$$\dot{\mathbf{q}}_h = (\mathbf{I} - \mathbf{J}^+ \mathbf{J}) \dot{\mathbf{q}}_0 \quad (4.23)$$

4.4.3 Comprehensive Solution

The comprehensive solution (Equation 4.24) of the pseudoinverse method is calculated by summing the special- and homogeneous solution. It describes the required cylinder velocities depending on the desired end-effector velocity and the current hydraulic cylinder positions \mathbf{q} since these are enclosed in the Jacobian matrix. The least norm solution can be modified through adding any nullspace solution by $\dot{\mathbf{q}}_0$.

$$\dot{\mathbf{q}} = \dot{\mathbf{q}}_{sp} + \dot{\mathbf{q}}_h = \mathbf{J}^+ \cdot \dot{\mathbf{q}}_d + (\mathbf{I} - \mathbf{J}^+ \cdot \mathbf{J}) \cdot \dot{\mathbf{q}}_0 \quad (4.24)$$

4.5 Gradient Projection Method

In this thesis, the gradient projection method is used to find an energy-saving and joint limit avoiding solution of the pseudoinverse method. This approach allows combining both requirements while having a great influence on the self-motion of the crane arm. In the following sub-chapters firstly a joint limit avoidance method is included in the gradient projection method, secondly, an optimization concerning a reduction of the volumetric flow rate is embedded and then this approach is modified to a reduction of energy consumption.

4.5.1 Joint Limit Avoidance

Similarly as introduced in Chapter 3.2.2.2 the nullspace vector $\dot{\mathbf{q}}_0$ of Equation 4.24 is replaced by the gradient of a performance criterion to avoid joint limits. This criterion is adopted from Chan et al.[8] and adapted to GPM in the same manner as it is proposed by Cheng [9]. The performance criterion $\mathcal{C}(\mathbf{q})$ is expressed in Equation 4.25 and its gradient is built as demonstrated in Equation 4.26.

$$\sum_{i=1}^3 \left(\frac{\partial \mathcal{C}}{\partial q_i} \right)^2$$

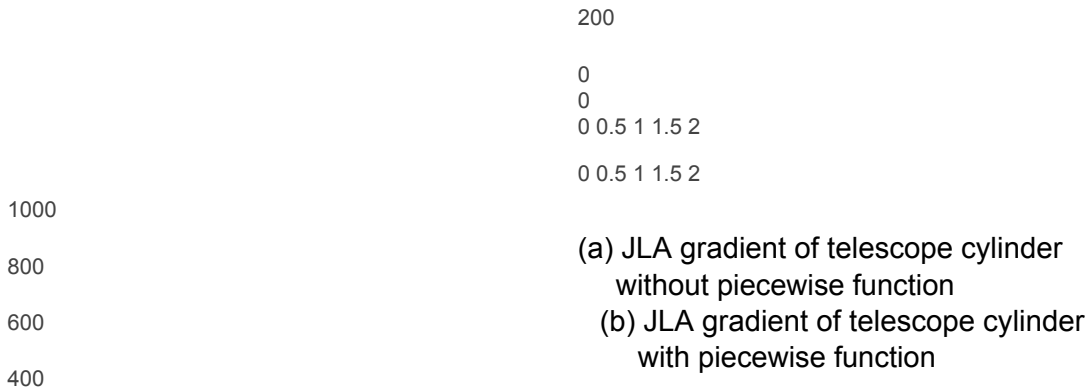


Figure 4.5: Variations of JLA gradient function of the telescope cylinder

The second point of optimization is a function similar to Equation 3.9 which was introduced by Chan et al.[8], in order to have no effect on the homogeneous solution \mathbf{h} , when the hydraulic cylinder is moving away from the joint limits, towards the center. For this, the approach of Chan et al. needs to be modified to be suitable for GPM instead of the

4.5 Gradient Projection Method

weighted pseudoinverse solution. This is achieved by building the difference quotient of the performance gradient separately for each row in respect to time. If the absolute value of the performance gradient of the actual time step is smaller than the one of the previous time step, this means the cylinder is moving towards the center. Hence, the value of the corresponding row of \mathbf{G} will be set to zero. For the contrary case, the value of \mathbf{G} stays the same. This can be seen in the following condition:

$$\begin{aligned}
 & \text{if } \Delta \mathbf{g}_i \geq 0 \\
 & \mathbf{G}_i = \mathbf{G}_i \\
 & \text{0, if } \Delta \mathbf{g}_i < 0 \quad (4.28)
 \end{aligned}$$

For the real machine operation algorithm, both modifications of the JLA are intertwined in "if" conditions and are queried every time step. The Matlab code describing these conditions can be found in the Appendix A.3

To ensure a suitable application of the JLA for all loading cycles, the weighting of the gradient $\Delta \mathbf{g}_i$ on the nullspace must be set correctly. This is done by setting the parameter \mathbf{w}_i to a sufficiently high value. At the same time, however, this value should be as small as possible in order to hinder optimization according to the minimum energy as little as possible. By iterative methods, the parameter \mathbf{w}_i is adjusted in such a way, that complete maneuverability in the workspace is guaranteed. The embedding of the JLA in the

inverse solution is shown in the following equation:

$$\mathbf{q} = \mathbf{J}^+ \cdot \mathbf{p} + (\mathbf{I} - \mathbf{J}^+ \cdot \mathbf{J}) \cdot \Delta \mathbf{q} \quad (4.29)$$

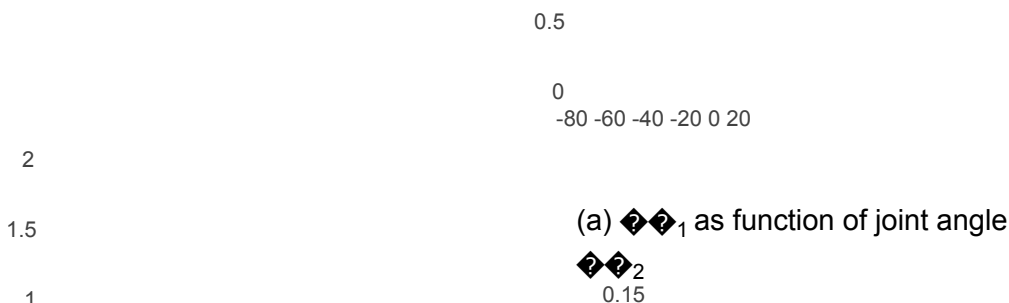
4.5.2 Volumetric Flow Rate Reduction

In Chapter 3.2.2.2 a flow reduction method elaborated by Cheng et al. [9] is introduced. This algorithm is adapted to the discussed knuckle-boom crane in this chapter. Therefore, in section 4.2, the joint angles are transformed to the hydraulic cylinder positions. This is a mandatory step to compute the volume flow consumed by each joint, depending on the joint motion. By looking at the results of transformation functions (Equations 4.7, 4.15), it is clearly seen that these transformation functions are not linear. The correlation of cylinder position q_1 as a function of q_2 is visualized as exemplary for joint q_2 in Figure 4.6a. Due to the nonlinear function, the volume flow is not constant over joint angle q_2 . This corresponds only to revolute joints actuated by linear hydraulic cylinders. In the case of the telescope cylinder, the function remains linear, just multiplied by $\frac{1}{2}$ because of the internal transmission of the telescoping section. Furthermore, since the hydraulic cylinders have different acting areas on the rod and piston sides, the volume flow also depends on the direction of motion. In [9] a flow consumption rate (FCR) is introduced, which describes these correlations. The FCR denotes the displaced volume of hydraulic

fluid by each joint angle. By multiplying the FCR with the angular joint velocity, the volumetric flow rate of the joint motion is computed. The FCR is denoted by the derivative

4 Methods

of the q_2 to q_1 transformation resolved to q_1 . The hydraulic volume is spanned by multiplying the acting area dependent on the direction of joint velocity onto the term. Since the FCR directly depends on the derivative of the correlation between joint angles to hydraulic cylinder positions, the FCR varies over the joint range. Also, the FCR in liter per degree of joint angle is visualized exemplary for joint q_1 over joint angle in degree (Figure 4.6b). In this figure, the negative joint velocity of q_2 is plotted. This function proves that volume flow is not only dependent on joint speed but also the position or range in which the joint operates. Both have an influence on the volume flow consumed. This states the importance of a volumetric flow reduction algorithm as a function of the cylinder positions.



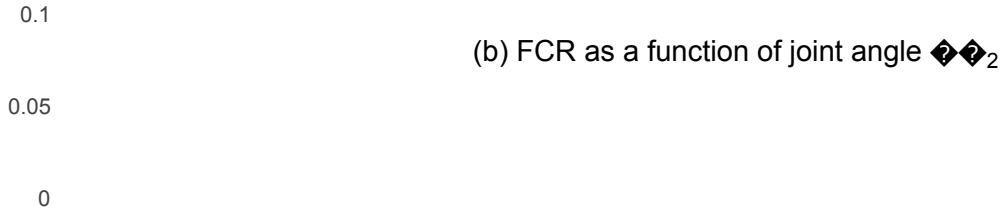


Figure 4.6: Cylinder position and FCR as a function of joint angle θ_2

Since the acting areas of the hydraulic cylinders vary dependent on the direction of joint velocity, piecewise functions describe the cylinder areas. Due to the underlying conventions of the Denavit-Hartenberg notation, an extending, an extending motion of the hydraulic cylinders acting on joints θ_2 and θ_3 , results in a negative joint velocity. The prismatic joint θ_4 acts in the same direction as its hydraulic cylinder. Furthermore, joint θ_2 differs from the remaining joints, because it is actuated by a single acting hydraulic cylinder. Hence, only volume flow must be supplied by the pump to lift the inner boom. While lowering, the potential energy of the crane arm is used to displace the oil in the hydraulic cylinder. The hydraulic cylinder of joint θ_3 and θ_4 are double-acting. Thus, the area of the piston and rod are taken into account. The piecewise function describing these correlations is expressed in Equation 4.30. $A_{r,c}$ stands for the rod side area and $A_{p,c}$ for the piston side area. The subscript c indicates the considered cylinder. The count is similar to the cylinder length n_c , which is always $n_c - 1$ to the depending joint θ_{n_c} .

40

$$\begin{aligned}
 & 0 \quad A_{r,1}, \quad 4.5 \text{ Gradient Method} \\
 & \text{if } \dot{\theta}_2 < 0 \\
 & \quad A_{p,2}, \text{ if} \\
 & \quad \dot{\theta}_3 \geq 0 \\
 & \quad A_{p,2}, \text{ if} \\
 & \quad \dot{\theta}_3 < 0 \quad \text{Projection} \quad (4.30) \\
 & \quad A_{p,3}, \text{ if} \\
 & \quad \dot{\theta}_4 \geq 0 \\
 & \quad A_{p,3}, \text{ if} \\
 & \quad \dot{\theta}_4 < 0 \\
 & 0, \text{ if } \dot{\theta}_2 \geq
 \end{aligned}$$

The performance criterion to minimize the volumetric flow rate is defined by the sum of the volumetric flow rates of each cylinder as a function of the cylinder area A_{c} and the cylinder velocity $\dot{\theta}_{n_c}$ (Equation 4.31). Equivalently it can be

said, that the performance criterion is a function of the FCR of each joint multiplied by the joint velocity. This distinguishes the method chosen in this thesis, from the method of Cheng et al. [9], since the transformation functions of the joint velocity to cylinder velocity are already included in the Jacobian matrix.

$$\sum_{i=1}^3 \mathbf{J}_{i, \dot{q}_i} = \mathbf{J}_{2, \dot{q}_2} \cdot \dot{q}_2 + \mathbf{J}_{3, \dot{q}_3} \cdot \dot{q}_3 \quad (4.31)$$

$$\mathbf{J}_{i, \dot{q}_i} = \mathbf{J}_{i, \dot{q}_i} \cdot \dot{q}_i +$$

The performance gradient reduces to the piston or rod side area of the corresponding hydraulic cylinder:

$$\Delta V = \sum_{i=1}^3 \mathbf{A}_{i, \dot{q}_i} \cdot \dot{q}_i \quad (4.32)$$

The magnitude of the performance gradient is crucial for the success of the optimization. For this purpose, a coefficient $\mathbf{C}_{i, \dot{q}_i}$ is used to trim the gradient to a suitable magnitude, similar to the JLA. As introduced by Cheng et al. [9] $\mathbf{C}_{i, \dot{q}_i}$ is designed as a low-adaptive coefficient matrix. This matrix consists of a parameter $\mathbf{C}_{i, \dot{q}_i}$ and a diagonal matrix of the current cylinder velocity (Equation 4.33). This guarantees direct feedback of the current volume flow as the cylinder velocity is a system response. The parameter $\mathbf{C}_{i, \dot{q}_i}$ sets the magnitude of the gradient and therefore, determines the influence of the gradient on the nullspace solution. With a greater magnitude, the efficiency of the algorithm maximizes and results in greater self-motion. The sign of $\mathbf{C}_{i, \dot{q}_i}$ needs to be set negative since this algorithm is a minimization problem. The motion of each joint and thus, the self-motion is limited by the maximal volumetric flow rate of each hydraulic cylinder. Due to different areas of the cylinder's rod and piston side areas, this value varies for every hydraulic cylinder and direction of motion. Euler et al. [13] conceived an algorithm to define the parameter $\mathbf{C}_{i, \dot{q}_i}$ for every time step. This approach computes $\mathbf{C}_{i, \dot{q}_i}$ to exploit the limits of self-motion while complying with

4 Methods

the performance criterion. The algorithm was introduced on a non-hydraulic robotic arm. Thus, no effects due to different cylinder areas or non-linear transformation functions between the joint variable and the cylinder variable are considered. Furthermore, no system variable like $\mathbf{C}_{i, \dot{q}_i}$ is included by Euler. Kaupp [24] implemented the discussed algorithm on an energy-solving approach and observed heavy oscillations caused by the variability of the parameter $\mathbf{C}_{i, \dot{q}_i}$. Since in this thesis the coefficient $\mathbf{C}_{i, \dot{q}_i}$ already contains a variable, it is decided against a continuous adjustment of the parameter $\mathbf{C}_{i, \dot{q}_i}$. This would distort the influence of the variable $\mathbf{C}_{i, \dot{q}_i}$ on optimizing the volumetric flow rate. Instead, an

iterative method is applied to find a constant parameter α that ensures stable operation of the algorithm while approaching optimal results. The iterative adaption of α is inspired by an algorithm introduced by Dubey et al. [35]. This algorithm finds a suitable parameter α in an iterative manner. In this approach, the joint velocities are calculated for one time-step and checked for meeting the boundary conditions. If the boundary conditions are exceeded, the parameter will be lowered. If not, α will be raised to a higher value. This leads to an approach to the optimal parameter. In the model investigated in this thesis, no clear boundaries are observed. By approaching the limit of an optimal condition the model resulted in high oscillations. Inserting a low-pass filter to the return signal of α helps to use higher values of α .

$$\begin{bmatrix} \alpha_1 & 0 & 0 \\ 0 & \alpha_2 & 0 \\ 0 & 0 & \alpha_3 \end{bmatrix} = \begin{bmatrix} \alpha_1 & 0 & 0 \\ 0 & \alpha_2 & 0 \\ 0 & 0 & \alpha_3 \end{bmatrix} \cdot \begin{bmatrix} \alpha_1 & 0 & 0 \\ 0 & \alpha_2 & 0 \\ 0 & 0 & \alpha_3 \end{bmatrix} \quad (4.33)$$

The performance gradient $\frac{\partial J}{\partial \alpha}$ and the corresponding low-adaptive coefficient α are included in the JLA method by adding both gradients and coefficients (4.34). The validity of this procedure is proofed by Cheng et al. [9].

$$\alpha = J^+ \cdot \alpha + (I - J^+ \cdot J) \frac{\partial J}{\partial \alpha} \cdot \Delta \alpha + \alpha \cdot \Delta \alpha \quad (4.34)$$

4.5.3 Energy Optimization

The hydraulic power consumed by each hydraulic cylinder P_i is composed of the volumetric flow and the pressure of each cylinder for each time instant. The overall power of the load sensing system P_{total} is a function of the sum of all volumetric flow rates and the highest cylinder pressure. This is a simplified consideration, as leakage and pressure losses through the system are neglected. The power consumed by each hydraulic cylinder and the power of the system can be computed as follows:

$$P_i = Q_i \cdot p_i = \sum_{i=1}^3 Q_i \cdot p_i \quad (4.35)$$

$$P_{total} = \sum_{i=1}^3 Q_i \cdot p_i \quad (4.36)$$

The energy consumption by the system over a time period $[t_0, t_f]$, is the integral of the instantaneous power over this time period:

$$E = \int_{t_0}^{t_f} P_{total} dt = \int_{t_0}^{t_f} \sum_{i=1}^3 Q_i \cdot p_i dt \quad (4.37)$$

In the following two sub-chapters, an approach to reduce the hydraulic energy consumption of the load sensing system is presented. This method is an extension of the volumetric ow optimization algorithm presented in Chapter 4.5.2.

4.5.3.1 Reduction of Hydraulic Power

In order to reduce the hydraulic power at each time step, the volumetric ow optimization algorithm must be extended by the hydraulic pressure. Therefore, the corresponding pressure of each hydraulic cylinder is chosen. The performance criterion dened in Equation 4.32 can be used unchanged and also its gradient ($\Delta \dot{V} = \Delta \dot{V}$). This is justified since this term is responsible for the optimization of the volumetric ow rate. The current cylinder pressure is incorporated in the ow-adaptive coefficient. For this purpose, it is directly integrated into the diagonal matrix. \dot{V} then becomes \dot{V} and resembles the Equation below:

$$\begin{pmatrix} \dot{V}_1 & 0 & 0 \\ 0 & \dot{V}_2 & 0 \\ 0 & 0 & \dot{V}_3 \end{pmatrix} = \begin{pmatrix} \dot{V}_1 & 0 & 0 \\ 0 & \dot{V}_2 & 0 \\ 0 & 0 & \dot{V}_3 \end{pmatrix} \cdot \begin{pmatrix} p_1 & 0 & 0 \\ 0 & p_2 & 0 \\ 0 & 0 & p_3 \end{pmatrix} \quad (4.38)$$

Multiplication by the pressure shifts the magnitude of the power optimizing gradient compared to the volumetric ow rate optimizing gradient. This can be compensated by adjusting the parameter \dot{V} . For this purpose, \dot{V} is set equal to \dot{V} and resolved after the parameter \dot{V} to be set. By inserting the values of pressure and ow rate of a representative operating condition, the new value for \dot{V} can be determined. This equation yields three solutions, one for each row of the matrix. The hydraulic cylinder with the biggest impact on energy consumption should be chosen for this purpose. The calculated value is only a suggestion and must be further optimized with the iterative adjustment algorithm according to Dubey et al. [35]. If necessary the low-pass filter also must be adjusted. In this thesis, a further low-pass filter is avoided for returning the actual hydraulic pressure. If necessary, further oscillations can be avoided by including a low-pass filter to the feedback pressure.

(a) Gradient ΔP_{opt} of cylinder 1 (b) Gradient ΔP_{opt} of cylinder 2

(c) Gradient ΔP_{opt} of cylinder 3

Figure 4.7: Power gradient ΔP_{opt} as a function of P and v

The previous steps form a performance gradient that is dependent on the current pressure and velocity of each hydraulic cylinder. This gradient, separately for each cylinder, is visualized in Figure 4.7. Thereby, the pressure P and the cylinder velocity v is displayed on the horizontal axes. The ΔP_{opt} axis rises from the right to the left for better visualization. The power optimizing gradient is plotted on the vertical axis. A bend of the linear curves for the velocity $v = 0$ is conspicuous. This is caused by the different areas for the piston and the rod side as expressed in Equation 4.30. For cylinder 1, the gradient is zero in the range of negative cylinder speeds, since this is a single-acting cylinder. The gradient rises to a minimum and maximum value for great pressure and great volumetric flow rate. These are the operation points with the greatest energy consumption. If the flow rate is positive, the gradient is maximal and vice versa. This contrary effect leads to self-motion

reducing these energy-intensive operation points.

The newly formed gradient can be included in the composite pseudoinverse solution in the same manner as the volumetric flow reduction gradient, by simply replacing it. This leads to the following notation of the JLA and the power optimal method of the pseudoinverse solution:

$$\dot{\mathbf{q}} = \mathbf{J}^+ \cdot \dot{\mathbf{v}} + (\mathbf{I} - \mathbf{J}^+ \cdot \mathbf{J}) \cdot \Delta \mathbf{q} + \mathbf{J}^+ \cdot \Delta \mathbf{v} \quad (4.39)$$

4.5.3.2 Influence of Pressure on Hydraulic Power

The volumetric flow rate of the system is a direct result of the system's kinematics since the only variable factor is the cylinder velocity $\dot{\mathbf{q}}$. Furthermore, the volumetric flow rate and thus, the resulting cylinder motion is a direct-control variable of the system and are regulated via the valve openings of the hydraulic control valves. The cylinder pressure is not a direct-controlled variable of the system and results from the system dynamics. The pressure is applied to the respective cylinders by external forces such as gravitational, Coriolis, and inertial forces. Hence, the hydraulic pressure is not directly controllable by only one control variable, instead, it results from joint configurations, velocities, and accelerations. This makes it hard to lower the system's pressure by having the cylinder velocity and position as the only control variable. To gain a greater influence on the pressure, the exponent α is introduced. This leads to the following equation of $\dot{\mathbf{q}}$:

$$\dot{\mathbf{q}} = \mathbf{J}^+ \cdot \dot{\mathbf{v}} + (\mathbf{I} - \mathbf{J}^+ \cdot \mathbf{J}) \cdot \Delta \mathbf{q} + \mathbf{J}^+ \cdot \Delta \mathbf{v} \quad (4.40)$$

Thereby α must be chosen similarly for all cylinders to not weight the cylinders differently. By changing the power α , the magnitude of $\dot{\mathbf{q}}$ changes as well. The parameter α must be adjusted in the same manner as explained in the previous sub-chapter. Furthermore, the same procedure as for optimizing the parameter α can be applied to find the optimal value of α .

In the following figure, a 2D and 3D presentation of the power optimization gradient for different exponents α of the pressure is presented in two graphs. The hydraulic cylinder 3 of the telescope joint is shown exemplarily. The left plot is a 2D plot and shows the power optimization gradients over the hydraulic pressure for the mentioned cylinder. This plot presents the instance of maximal volumetric flow rate since the effects of the exponent are the clearest to see. On the right side, the 2D plot is extended over the full range of the cylinder velocity. The gradient is visualized for three different powers of the pressure ($\alpha_3=1$ =yellow, $\alpha_3^{1.5}$ =red, α_3^2 =blue). The three lines don't all cross in one point, because the parameter α is adjusted according to the lift cylinder. This scenario is caused by differentiating cylinder velocities due to different cylinder areas. Nevertheless, it is clearly visible, that for low-pressure sectors the gradient decreases with increasing potency.

4 Methods

For high pressures, a rapidly increasing nonlinear response can be seen with increasing potency. This promises very good feedback in order to mitigate the hydraulic operating points with high energy consumption since low pressures are less penalized but higher pressures more so.

(a) Gradient $\Delta P_{3,3}$ of cylinder 3 (b) Gradient $\Delta P_{3,3}$ of cylinder 3

Figure 4.8: 2D and 3D plot of the power gradient $\Delta P_{3,3}$ as a function of $P_{3,3}$ and $P_{3,3}$ for different potencies

4.6 Inclusion of Hydraulic Transformer

In Chapter 3.2.1 a hydraulic transformer as a further energy saving component is presented and its hydraulic operating principle is discussed. In order to enhance further energy savings, this hydraulic transformer is included in the previously presented algorithms. The transfer of energy between joint $P_{2,2}$ and $P_{3,3}$ can be incorporated directly into the pseudoinverse solution. For this purpose, Kaupp [24] has presented a solution to integration the characteristics of the hydraulic transformer directly into the Jacobian matrix. The hydraulic transformer consists of two pumps/motors each connected to hydraulic cylinder 1 and cylinder 2. These motors/pumps are coupled mechanically and thus, result in the same rotational speed. The two motors/pumps have the same displacement. Hence, the same volumetric flow rate is conveyed. Due to different piston areas, this results in different cylinder velocities $V_{1,1}$ for each cylinder. This correlation is expressed in Equation 4.41. By solving this term to velocity $V_{1,1}$, the additional cylinder velocity due to the transformer is expressed for cylinder 1 (Equation 4.42). [24]

4.7 Integration of inverse solution in simulation model

$$\begin{aligned}
 \dot{V}_{1,hydraulic} &= \dot{V}_{2,hydraulic} \\
 \dot{V}_{1,hydraulic} \cdot A_{1,hydraulic} &= \dot{V}_{2,hydraulic} \cdot A_{2,hydraulic} \quad (4.41) \\
 \dot{V}_{1,hydraulic} &= \dot{V}_{2,hydraulic} \cdot \frac{A_{2,hydraulic}}{A_{1,hydraulic}}
 \end{aligned}$$

Since a part of the required volume flow, to meet the required joint velocity $\dot{\theta}_1$ results from the hydraulic transformer ($\dot{V}_{1,hydraulic}$), the part of the velocity resulting from the volume flow provided by the pump (\dot{V}_1^*) has to be adapted. The requested cylinder velocity \dot{V}_1 depends only on the driver input and the kinematics and thus remains unchanged. Only \dot{V}_1^* has to be adjusted to compensate the hydraulic transformer. This is presented in Equation 4.43. [24]

$$\begin{aligned}
 \dot{V}_1 &= \dot{V}_1^* + \dot{V}_{1,hydraulic} = \dot{V}_1^* + \frac{A_2}{A_1} \cdot \dot{V}_{2,hydraulic} = \dot{V}_1^* \\
 &\quad + \frac{A_2}{A_1} \cdot \dot{V}_2 \cdot \frac{A_1}{A_2} \quad (4.43)
 \end{aligned}$$

The constant $\frac{A_2}{A_1}$ is inserted into the Jacobian matrix to adapt the forward kinematics in order to include the hydraulic transformer. $\frac{A_2}{A_1}$ consist of the corresponding cylinder areas of hydraulic cylinder 1 and 2. The product of $\frac{A_2}{A_1}$ and the first column is added onto the second column of the Jacobian matrix. The forward kinematics under consideration of the hydraulic transformer is presented in Equation 4.44. The pseudoinverse can be formed regularly by just using the new variation of the Jacobian matrix $J_{hydraulic}$. [24]

$$\begin{aligned}
 & \begin{bmatrix} \dot{\theta}_1 \\ \dot{\theta}_2 \end{bmatrix} = J_{hydraulic} \cdot \begin{bmatrix} \dot{V}_1^* \\ \dot{V}_2 \end{bmatrix} \quad (4.44) \\
 & J_{hydraulic} = \begin{bmatrix} \frac{A_1}{A_2} \dot{\theta}_1 & \dot{\theta}_2 \\ \dot{\theta}_1 & \dot{\theta}_2 \end{bmatrix} \\
 & = J_{kinematic} \cdot \begin{bmatrix} \dot{V}_1^* \\ \dot{V}_2 \end{bmatrix} \\
 & \begin{bmatrix} \dot{\theta}_1 \\ \dot{\theta}_2 \end{bmatrix} = \begin{bmatrix} \frac{A_1}{A_2} \dot{\theta}_1 & \dot{\theta}_2 \\ \dot{\theta}_1 & \dot{\theta}_2 \end{bmatrix} \cdot \begin{bmatrix} \dot{V}_1^* \\ \dot{V}_2 \end{bmatrix}
 \end{aligned}$$

4.7 Integration of inverse solution in simulation model

In previous work, a simulation model of the working hydraulics was developed [16]. This model is built in the simulation software Simulink Matlab. A schematic visualization of the simulation model is presented in Figure 4.9. The model contains all hydraulic correlations of the working hydraulics. Furthermore, the kinematics and dynamics of the crane arm are embedded in the system. This

allows a realistic simulation of working cycles considering all hydraulic and mechanical parameters. The input to the system is the velocity of the end-effector. According to the input, the corresponding cylinder velocities are computed in an energy minimal form, by the pseudoinverse solution developed in this thesis. To compute this solution, feedback of the hydraulic system is given by the position, velocity, and pressure corresponding to each hydraulic cylinder. The input \dot{q}_1 , which controls the slewing motion executed by joint 1 , is directly forwarded to the working hydraulics, since this joint works independent of the remaining and linear to the operator's input. A

4 Methods

visualization of the source code (Appendix A.3) for integrating the energy optimal solution and a glimpse into the realization in Simulink Matlab is presented in the Appendix A.2.

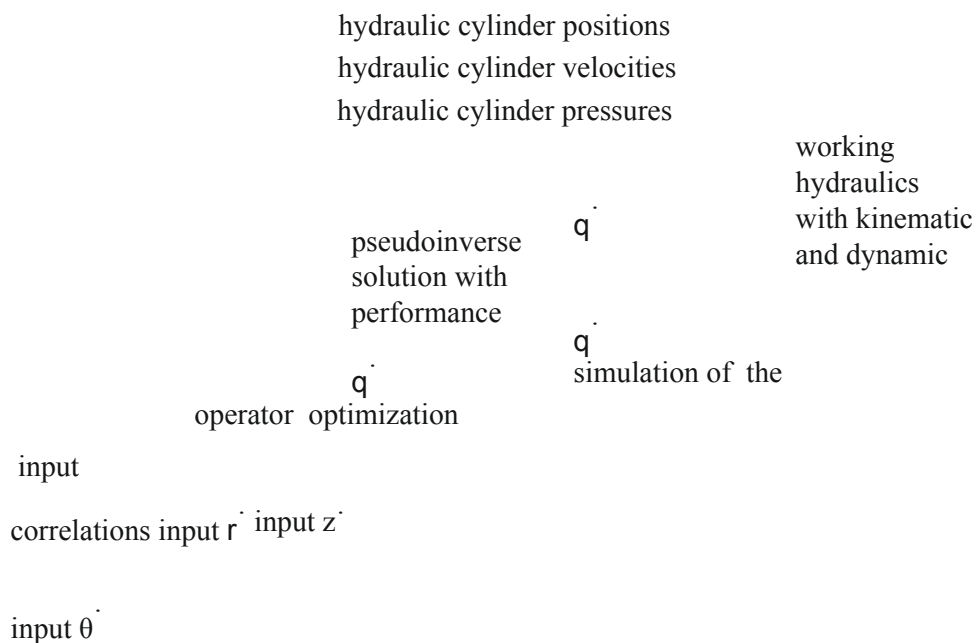


Figure 4.9: Schematic representation of the integrated inverse solution in a simulation model

5 Evaluation

In this chapter previously introduced algorithms are validated and discussed. Thereby, two main algorithms are distinguished. The optimization of volumetric flow rate and the optimization of hydraulic power in variation of the exponent are presented and compared. These algorithms are validated by performing three different test cycles for two variations of speed. Furthermore, the system is tested with and without the hydraulic transformer, and the influence of the HT on the effectiveness of the optimization algorithms is discussed. In the first sub-chapter, the results are presented and discussed in the following sub-chapter.

5.1 Results

The results of the energetic investigations are subdivided into the behavior of the system along three trajectories. These are explained in the first sub-chapter. In the second sub-chapter, the general conditions under which the results are investigated are stated. Subsequently, the outcomes of the inquiries are presented separately for each trajectory.

5.1.1 Test Trajectory

In a former thesis, [24] three trajectories have been defined. These represent common loading processes of a knuckle-boom crane in the full range of the

workspace. The presented trajectories only cover two dimensional motions in \hat{R} and \hat{Z} direction, since the slewing motion in Θ direction is independent of the remaining axes and thus, is irrelevant for the presented algorithms. The trajectories are divided into a horizontal (h), a vertical (v), and a diagonal (d) motion of the end-effector. Each trajectory consists of two sections, in which the crane arm is extended and retracted along a linear path. In the first section, the motion is paused for 3 s between the change of direction. In the second section, the direction is changed instantly. These two sections are also separated by a pause of 3 s. Furthermore, the system rests for 5 s before section one, to generate an initial idle state. The trajectories are operated at two different speeds. Hereby, the velocity vectors in \hat{R} and \hat{Z} direction have a magnitude of either 0.5 m/s or 1 m/s. In Figure 5.1 the three trajectories are visualized as a function of the end-effector position over time, for a velocity of 0.5 m/s along the corresponding axes. [24]

5 Evaluation

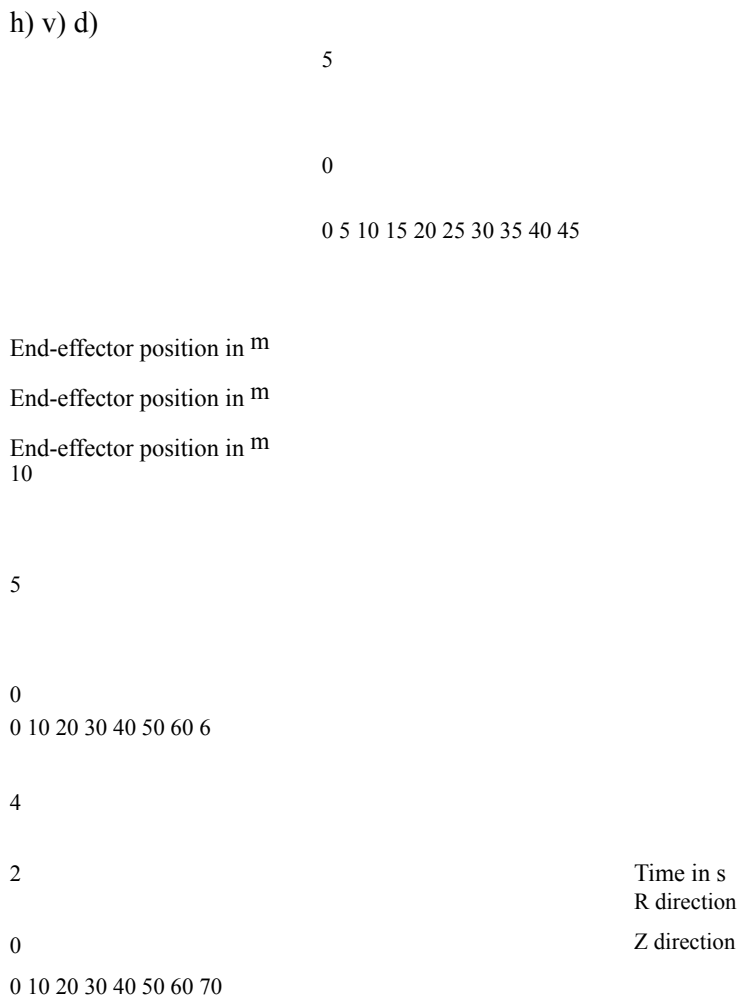


Figure 5.1: Test trajectories for slow horizontal, vertical, and diagonal cycle, adapted from [24]

Horizontal Trajectory To generate this trajectory, the velocity input along the \hat{R}

axis is set either to $0.5 \frac{m}{s}$ or $1 \frac{m}{s}$. The velocity along the x axis is set to $0 \frac{m}{s}$. For the velocity of $0.5 \frac{m}{s}$, this results in an extending motion of the end-effector for the time periods $5 \text{ s} - 17 \text{ s}$ and $35 \text{ s} - 47 \text{ s}$. The retracting motion proceeds during the time intervals of $20 \text{ s} - 32 \text{ s}$ and $47 \text{ s} - 59 \text{ s}$. [24]

Vertical Trajectory To generate this trajectory, the velocity input along the z axis is set either to $0.5 \frac{m}{s}$ or $1 \frac{m}{s}$. The velocity along the x axis is set to $0 \frac{m}{s}$. Due to the boundaries of the workspace, this trajectory needs an extra motion in x direction, before the main work period. Afterward, for the velocity of $0.5 \frac{m}{s}$, the input results in a lifting motion for the time periods $11 \text{ s} - 23 \text{ s}$ and $41 \text{ s} - 53 \text{ s}$. The lowering motion proceeds during the time intervals of $26 \text{ s} - 38 \text{ s}$ and $53 \text{ s} - 65 \text{ s}$. [24]

Diagonal Trajectory To generate this trajectory, the velocity input along the x and z axis are set either to $0.5 \frac{m}{s}$ or $1 \frac{m}{s}$. This results in a velocity of $0.71 \frac{m}{s}$ or $1.41 \frac{m}{s}$, because of the vectorial sum of the velocities. Due to the boundaries of the workspace, also this trajectory needs an extra motion in x and z directions, before the main work period. For the velocity of $0.5 \frac{m}{s}$, this results in an extending motion of the end-effector for the time periods $11 \text{ s} - 17 \text{ s}$ and $29 \text{ s} - 35 \text{ s}$. The retracting motion proceeds during the time intervals of $20 \text{ s} - 26 \text{ s}$ and $35 \text{ s} - 41 \text{ s}$. [24]

For the trajectories with the velocity of $1 \frac{m}{s}$, the motion time in each section is halved, to ensure the same path.

5.1.2 Simulation Results

The performance-optimizing algorithms presented in Chapter 4 are evaluated according to their energy reduction performance along the predefined test trajectories. These algorithms are tested in the simulation model presented in Chapter 4.7. As a reference condition, the least norm pseudoinverse solution, including a joint limit avoidance through gradient projection method (Chapter 4.5.1) is designated. The JLA is necessary to successfully follow the trajectories without reaching the joint limits. The algorithm for optimal volumetric flow rate (Chapter 4.5.2) and for optimal power (Chapter 4.5.3) are compared to the reference condition. In both, the JLA is implemented. The power optimal method is tested in three variations of the exponent ($\alpha = 1$, $\alpha = 1.5$, $\alpha = 2$). The algorithms are tested on a hydraulic system including the hydraulic transformer (Chapter 4.6) and are compared to a conventional system without the HT.

To generate static test conditions, the parameter Δ_{JLA} of the joint limit avoidance is set equally for all algorithms to $\Delta_{\text{JLA}} = -0.005$. The JLA includes the piecewise function, which sets the Δ_{JLA} to zero when the

joint is distant to the cylinder limits by more than 15% (Figure 4.5b). The second exception, which sets ΔP_{pump} to zero when the joint is moving towards the center (Equation 4.28), is not implemented for this test, because oscillation occurs when switching directions, which leads to incomparable conditions. The parameter α is set to $\alpha = -800$ for the volumetric flow rate optimization method. In the power optimizing method, α is set according to the exponent β . For $\beta = 1$ the parameter $\alpha = -0.0001$, for $\beta = 1.5$ the parameter $\alpha = -0.000000036$ and for $\beta = 2$ the parameter $\alpha = -0.00000000012$.

For the optimization algorithms, a low-pass filter is inserted to the feedback signal P_{pump} of the hydraulic system. The low-pass prevents the system of oscillations due to the direct feedback by smoothing P_{pump} . Furthermore, a control algorithm developed in a former thesis [24], ensures correct trailing of the trajectory.

The energy consumed over one test cycle is computed by integrating the hydraulic power demanded by the system. The hydraulic power is computed by multiplying the volumetric flow rate of the pump Q_{pump} and ΔP . The pressure ΔP is the pressure difference of the system's pressure to tank pressure. This leads to the following equation:

$$E_{cyc} = \int_0^{t_{cyc}} P_{pump} dt = \int_0^{t_{cyc}} Q_{pump} \Delta P dt \quad (5.1)$$

To compare the energy consumption between the algorithms the percentage of consumed energy per cycle is expressed in relation to the reference condition (solely JLA). In the following equation, $E_{cyc,ref}$ is the consumed energy of the reference condition, and $E_{cyc,alg}$ indicates the energy consumption of an optimization algorithm:

$$\% \text{ Energy Savings} = \frac{E_{cyc,ref} - E_{cyc,alg}}{E_{cyc,ref}} \cdot 100\% \quad (5.2)$$

The following results are presented in three bar diagrams (Figure 5.6, Figure 5.7, Figure 5.8), one for each trajectory. In each diagram, the absolute energy consumption over the tested trajectory is visualized in the first row. In the second row, the percentage of energy savings in comparison to the reference condition is presented. Each row is divided into two sub-sections. These sub-sections distinguish by the speed of motion. In the

first one, the trajectory has a velocity of $0.5 \frac{m}{s}$ along the x or y axes and is named slow cycle. The fast cycle presents the trajectories with a velocity of $1 \frac{m}{s}$. For each sub-section, the conventional system is compared to the system including the hydraulic transformer. Through the first bar, the reference

condition (JLA) is represented, for each cycle. In the second row of each diagram, this bar is 0 %, since it is the one compared to. The second bar represents the optimization of the volumetric flow rate (Q-optimal). The three remaining bars all depict the power optimal algorithm with a different exponent of the feedback pressure α . Hereby the exponent rises from the left to the right in increments of 0.5, starting with $\alpha = 1$. Additionally the same results are presented in Table 5.1. The same structure as for the bar plot is used to sort the results.

Horizontal Trajectory

In Figure 5.2 the energy consumption along the horizontal trajectory is presented. All results are compared to the performance of the reference algorithm (JLA) for each test cycle. The reference algorithm consumes less energy for the slow cycles than for the fast cycles. Furthermore, the system including the hydraulic transformer, compared to the conventional system consumes less energy for both velocities. Exact values are presented in the first third of Table 5.1. By comparing the volumetric flow rate optimization algorithm to the reference algorithm, the energy consumption of the conventional system is significantly higher for both velocities. 12.2 % and 14.6 % more energy is needed for the slow and fast cycle. The system with the HT achieves better results, as for the slow cycle 1.7 % is saved. The Q-optimal algorithm during the fast cycle consumes 2.7 % more energy than the reference cycle. The three variations of the power optimizing algorithm all consume less energy than the reference cycles and less than the Q-optimal cycle. Furthermore, for rising exponents the energy savings increase. The greatest energy saving occurs with the HT system for the fast cycle. In this case, 17 % energy can be saved in comparison to

the reference. The algorithm with the conventional system achieves assimilable energy savings (16 %) for the fast cycle. In the slow test cycle, the P-optimal algorithm saves more energy in combination with the conventional system, than with the HT-system, for an exponent of 1.5 and greater. The absolute energy consumption for the conventional system is higher, though. Concerning the P-optimal algorithm in conclusion can be said, that with higher velocity the energy-saving potential is greater. When comparing same velocities, the HT system consumes less energy than the conventional system.

Figure 5.2: Energy consumption of one horizontal cycle for different methods

Vertical Trajectory

The results of the tested algorithms on the vertical trajectory are presented in Figure 5.3. The exact values of this plot are presented in the second third of Table 5.1. The

5 Evaluation

energy consumption of the reference algorithm (JLA) is greater for the higher velocity. In contrary to the horizontal trajectory, the energy consumption of the system with the HT is higher compared to the conventional system. This trend also is apparent for the Q-optimal algorithm. By comparing both, the Q-optimal algorithm consumes more energy, except for the conventional system during the fast cycle. The P-optimal algorithm saves energy in all three variations of the exponent. Similar to the horizontal trajectory, the energy savings increase with rising exponent. The energy savings for the conventional system are greater than for the HT system. Also, similar to the horizontal trajectory, the energy savings of

all algorithms are greater for higher velocity. Therefore, the P-optimal algorithm with $\alpha = 2$, applied on at the conventional system during the fast cycle saves the most energy. With a value of 26.9 % this is the greatest energy saving of all trajectories.

Figure 5.3: Energy consumption of one vertical cycle for different

methods 54

5.1 Results

Diagonal Trajectory

Figure 5.4 presents the results of the tested algorithms on the diagonal trajectory. This trajectory is a combination of both previously shown trajectories. Thus, the results also have similarities to both. Similar to the horizontal trajectory, the reference algorithm consumes more energy in the conventional system. Also, for the fast cycles, more energy is consumed.

Figure 5.4: Energy consumption of one diagonal cycle for different methods

It must be said, that the reference algorithm (JLA) of the conventional system during the fast cycle is not able to follow the path in the $\diamond\diamond$ direction. This is caused by reaching the limits of volumetric flow rate at hydraulic cylinder 1. As it can be seen in Figure 5.5, the end-effector is not lowered to the full range of $\Delta\diamond\diamond$, which results in lower potential energy per cycle. Hence, the consumed energy of this cycle is expected to be higher for a correct

5 Evaluation

trailing of the path. Also, less volume flow is needed since the cylinders extend less. Since the remaining algorithms follow the path sufficiently well during this cycle, this leads to the assumption, that the percentage of energy saving for the other algorithms would be greater for a correct trailing of the reference algorithm. Therefore, the energy savings of the explicit cycle are not further mentioned. The trailing in along the R-coordinate is sufficiently near as visualized in Figure 5.5. The Q-optimal algorithm consumes more energy than the reference algorithm in

the conventional system. Although, the additional energy only is 0.2 % for the HT system in the fast cycle. With one exception, the variations of the P-optimal algorithm consume less energy than the reference in each cycle. Only for the power $\alpha = 1$, during the slow cycle in the HT system, more energy than the reference is consumed. With a higher exponent, the energy savings increase. The greatest energy savings of 24.3 %, are achieved in the HT system during the fast cycle. Also, the absolute consumed energy is lower for each algorithm in the HT system. This holds true for both velocities.



Figure 5.5: R-coordinate and Z-coordinate trailing of diagonal trajectory for fast cycle with conventional system

By comparing all three trajectories, it is shown, that the same system needs more energy for higher velocities. Furthermore, if only the same systems are compared, the energy saving potential is greater with higher velocity. The HT system consumes less energy during the horizontal and diagonal trajectory. This statement is not valid for the vertical trajectory. The P-optimal algorithm consumes less energy with rising exponent, except for one cycle of the diagonal trajectory. By only comparing same system types, the power optimization reduces the consumed energy up to 26.9 % on a conventional system during a vertical trajectory. When also comparing system types with each other, the greatest

energy savings can be found. In this case, the HT-system with the P-optimal algorithm consumes up to 31.8 % less energy, than the reference algorithm on a conventional system on a horizontal trajectory. In almost all cycles, besides two exceptions, the Q-optimal algorithm consumes more energy than the reference.

Table 5.1: Energy consumption of all three trajectories, absolute values and percentage of energy savings.

trajectory	cycle speed	trajectory	Energy consumption and savings																	
			no HT	HT	no HT	HT	no HT	HT	no HT	HT	no HT	HT								
			Energy [kJ]	Energy [kJ]	Savings [%]	Energy [kJ]	Energy [kJ]	Savings [%]	Energy [kJ]	Energy [kJ]	Savings [%]	Energy [kJ]	Energy [kJ]	Savings [%]						
0.5	h	no HT	664	745	-12.2	650	2.1	611	8.0	595	10.4	544	535	1.7	524	3.7	509	6.4	502	7.7
			no HT	801	918	-14.6	749	6.5	673	16.0	673	16.0	662	680	-2.7	600	9.4	570	13.9	546
0.5	v	no HT	376	387	-2.9	317	15.7	312	17.0	312	17.0	372	415	-11.6	369	0.8	350	5.9	338	9.1
			no HT	454	442	2.6	351	22.7	341	24.9	332	26.9	462	485	-5.8	414	10.4	389	15.8	373
0.5	d	no HT	573	606	-5.8	522	8.9	476	16.9	453	20.9	426	468	-9.9	437	-2.6	417	2.1	404	5.2
			no HT	605	674	-11.4	588	2.8	556	8.1	532	12.1	600	601	-0.2	501	16.5	474	21.0	454

5 Evaluation

5.2 Discussion

In order to build a better understanding of the impact of the algorithms on energy consumption, some aspects are discussed in more depth, in this chapter.

Energy Reduction Through P-Optimal Algorithm

Since this thesis searches for a minimal energy algorithm, the discussion firstly focuses on the power optimization algorithm in its three variations. To understand the operating principle of the algorithm, the volumetric flow rate and the pressure measured at the pump, must be contemplated to understand the operating principle of the algorithm. Since the power and thus, the energy is a function of these two parameters, these two functions are visualized in the top row of Figure 5.6. The resulting power and energy of the system are plotted in the bottom row. The reference algorithm is displayed as a blue line, whereas the power

optimization algorithm is displayed in red. For this comparison, the power optimization algorithm of power 2 is chosen. The displayed test cycle is the diagonal trajectory for the fast cycle and the conventional system.

Figure 5.6 confirms, that the P-optimal algorithm has a positive influence on the volumetric flow rate, as well as on the pressure of the system. The algorithm lowers the peaks of the volumetric flow rate successfully over a significant time range of the trajectory. Especially during the extending motion of the crane arm, the volumetric flow rate is lowered significantly. At the first peak ($\dot{V} = 5 \text{ dm}^3/\text{s}$) oscillations occur. These always have a negative influence on the effect of the optimization. Thus, the energy consumed is higher for this peak. Due to the direct feedback of the cylinder velocity and the cylinder pressure, these oscillations have a direct impact on the feedback matrix \mathbf{K}_{FB} . With greater parameter α the oscillations increase due to feedback effects. These effects are greater for the cylinder velocity than for the pressure since the cylinder velocity is a direct control variable of the system.

The effects on the reduction of pressure peaks are even greater than on the volume flow. Figure 5.6b shows, that the maximum pressure over the whole cycle is reduced by 27%. In sections of lower pressure, the pressure rises. The higher pressure is caused by different joint configurations of the crane arm in comparison to the reference cycle. The highest load sensing pressure is set by a different cylinder due to the algorithm. This effect mostly does not have a negative impact on the energy consumption of the system, since often in these areas the volumetric flow rate is zero. In Figure 5.7, the pump pressure of the same cycle is plotted for a variation of all three tested exponents. With a higher exponent, the pressure peaks decrease. The theoretical effects of the exponent on the performance gradient are presented in Chapter 4.5.3.1. These are mirrored in the simulation. In sections of high pressure, the algorithms with greater exponent achieve a major reduction of pressure, whereas in low-pressure areas the pressure rises with a higher exponent. With rising exponent, the pressure magnitude is distributed more equally over the trajectory, since high- and low-pressure peaks are equalized out. This is a deliberate effect in order to reduce energy consumption. Especially during the extending motion, a major reduction of power can be observed, of up to 50%. This is visualized in Figure 5.6c.

(a) Pump volumetric flow rate over time (b) Pump pressure over time

(c) Power over time (d) Energy over time

Figure 5.6: Comparison of pump parameters of JLA and P-optimal power 2 algorithm for conventional system on (d) trajectory (see Figure 5.1) in fast cycle

The exponents chosen for this evaluation are only examples. In most cycles, the energy savings rise with each increase of the power n . Only in few cases, these energy savings stagnate for exponent $n = 2$. This leads to the assumption, that for further increase of the exponent, the energy savings will rise for most cycles. In an iterative process, an optimal condition can be approximated. This process copes with certain difficulties since, with every change of the exponent n , the parameter k must also be adjusted to an optimal condition in multiple iterations. Furthermore, the optimal exponent n can be approximated to a certain extent since, for each trajectory and velocity, the system reacts differently.



Figure 5.7: Comparison of pressure reduction for various exponents α of P-optimal algorithm

Influence of Cycle Velocity on Energy Consumption

When comparing the energy consumption due to the cycle speed, it can be seen that the fast cycle always consumes more energy for the same path. A greater velocity of the end-effector results in a greater velocity of the hydraulic cylinders and thus, the volumetric

flow rate is higher. The same effect can be seen for the pressure. The pressure is a function of the forces applied to the system. These forces are dependent on velocity and acceleration. Higher velocities also result in higher acceleration, since the trajectory velocities are constant for most of the time and have a ramp form for each change of velocity. The power optimization algorithm achieves greater energy saving for the fast cycles. This can be explained by the fact, that for higher velocities the peaks of pressure and volume flow are more intense. Hence the previously explained attenuating effects of the algorithm have a greater impact. This leads to a greater decrease of energy consumed by the system.

Problems Concerning the Q-Optimal Algorithm

For most cycles, the energy consumed by the Q-optimal algorithm is higher than by the reference algorithm. Firstly must be stated, that the reference algorithm already is the least norm solution with respect to minimum hydraulic cylinder velocities. That means the non-linear relation, discussed in Chapter 4.5.2 and presented through the FCR, is already taken into account. The Q-optimal algorithm only distinguishes through a vector that consists of the cylinder areas. These cylinder areas weight the motion and direction of

motion of each cylinder differently and hence, change the magnitude of the FCR by a constant factor.



Figure 5.8: Comparison of Volumetric flow rate for Q-optimal algorithm and reference algorithm

To further discuss the performance of the Q-optimal algorithm, this algorithm is compared to the reference algorithm in Figure 5.8. The volumetric flow rate is plotted for both of them, for the (h) trajectory of the conventional system performing a fast cycle. Similar to the P-optimal algorithm, the Q-optimal algorithm successfully lowers the peaks of each section. In the test simulations of the Q-optimal algorithm increased oscillations occur. In Figure 5.8 this can be seen, at the peak of the volumetric flow rate during the retracting motions of the crane arm. These oscillations occur due to a poorly adjusted parameter ζ and the according low-pass filter. The feedback cylinder velocity of the hydraulic system is a direct control variable of the algorithm, which leads to back coupling oscillation effects. The oscillations aggravate the search after low volumetric flow rates, for the algorithm, since no clear feedback is given. In the visualized cycle, immediately after the oscillations decay, an increase of volume flow can be observed, for example during the time intervals 15-20 and 30-35. This phenomenon can be explained by these aggravated conditions for the algorithm due to oscillating feedback. Better adjustment of the parameter ζ and correspondingly a suitable setting of the low-pass filter, will reduce oscillations and can produce better results. This can be seen in the test of the P-optimal algorithm since this algorithm only is an extension of the Q-optimal algorithm. For the cycle, presented in Figure 5.6c, the volume flow is reduced effectively, while only few oscillations occur.

An additional problem is, that this algorithm does not search for a global optimum. Explicitly in this cycle, this could explain the poor performance. Hydraulic cylinder 1 is single-acting and therefore while retracting has no effect on the volumetric flow rate.

5 Evaluation

While extending the crane arm, cylinder 1 is retracted as far as the joint limit avoidance allows. In contrast, while extending cylinder 1 again for the contrary motion of the crane arm, a major volume flow is needed due to the large cylinder area. Hence, this motion is

mostly avoided by the Q-optimal algorithm. Due to the joint limits of the remaining joints and limitations of possible joint configurations, the trajectory can not be realized without a motion of cylinder 1. This leads to an inevitable extending motion of the cylinder in configurations with poor performance. The discussed issue explains why during the time period 5 s - 12 s the volume flow consumption of the Q-optimal algorithm is similar or less than the reference cycle. For repeating the same motion during the time interval 23 s - 28 s, the start conditions are different, due to a total retract of the IBC during the first period. This leads to a worse volume flow consumption in the second period.

Likely a combination of both problems presented leads to the poor results of this algorithm. Apart from this, this algorithm is not expected to reduce energy, since it only searches for low volumetric flow rates.

Performance of the HT System in Collaboration with the P-Optimal Algorithm

The results prove, that the inclusion of the hydraulic transformer into the power optimization algorithm is accomplished successfully. Especially the horizontal trajectory is favorable for the HT-system. During the fast cycle, the P-optimal, power 2 algorithm saves 19 % more energy in the HT-system, compared to the same algorithm in the conventional system. This effect occurs due to the contrary motions of the inner and outer boom during a horizontal motion of the end-effector. The potential energy of the booms can be transformed, while one boom is lowering and the other is raising. This is used by the algorithm by preferring this motion.

The vertical trajectory in contrast is not favorable for the HT system. The test cycles of this trajectory mostly lead to higher energy consumption of the HT system compared to the conventional system. During this trajectory, the inner and outer boom mainly both raise or lower at the same time. No potential energy can be transferred. Hence, the coupling of the inner and outer boom is rather hindering the algorithm.

Since the diagonal trajectory is a combination of the horizontal and the vertical trajectories, both cases can be observed. In this case, the absolute energy consumed by the HT-system is greater, than by the conventional system. Whereas the percentage energy savings of the P-optimal algorithm are greater for the conventional system. Since the algorithm can not in all cases prefer a contrary motion of the inner and outer boom, in the remaining cases the coupling can be hindering.

Problems Due to Oscillations

The algorithms presented are very vulnerable to oscillations. On the one hand oscillation emergence for a great parameter of ω , due to the direct feedback from the hydraulic system of cylinder velocity and pressure. On the other hand, these oscillations have a negative effect on the effectiveness of the

algorithm. Especially the feedback of the cylinder velocity has a great impact on oscillations of the system. A low-pass filter helps to reduce these. The interplay of the low-pass filter and the parameter α is very sensible. Hence,

to set a test environment that is comparable for all systems and algorithms, the factor α in combination with the low-pass filter is rather set to moderate conditions. For each system and algorithm, this can be done separately in an iterative manner, instead of having one overall condition. This would improve the energy consumption of each algorithm individually.

As stated in Chapter 5.1.2, in all tested cycles, the joint limit avoidance was not set to zero for a cylinder motion towards the center as explained in Chapter 4.5.1 (Equation 4.28). This decision was made due to problems with oscillations for changing directions of motion. This step is valid since due to the GPM, the JLA gradient adds a velocity with opposite direction onto the corresponding joint through the homogeneous solution. If the JLA proportion of velocity was set to zero immediately after the joint is stopped before reaching the joint limit, the joint could continue towards the joint limit. Then, because of a velocity towards the joint limit, the JLA is active again until the joint changes direction. This procedure repeats and leads to an oscillation.

In contrast, having a JLA when not absolutely need can limit the effectiveness of the energy optimizing algorithm. One way of solving this problem is including a delay time before turning the gradient to zero after the direction of motion is changed towards the center. This time-dependent method can be implemented in addition to the already existing cylinder position-dependent method of turning JLA to zero when not necessary (Figure 4.5b). This time-dependent method guarantees, that due to a longer influence of the JLA and hence a greater distance to the joint limit, the influence of the velocity due to the JLA is sufficiently small when turned to zero, to not result in a change of velocity direction. Also, this time period is dependent on the system and algorithm. When this condition is set correctly the impact of the JLA on the nullspace solution can be reduced. This increases the influence of the energy optimizing algorithm on self-motion and leads to greater energy reduction.

Limitation of Energy Reduction Through Local Solution

All presented algorithms search for optimal conditions regarding their particular performance criterion for each instant. This does not necessarily lead to an optimal condition over the complete trajectory, since each instance is not compared to the previous and following instant. These effects have already been discussed for the Q-optimal algorithm. Since the P-optimal algorithm is an extension of the Q-optimal algorithm, it is shown that this algorithm as well would profit from a global solution. Also, the optimization in relation to the HT-system could profit from a global solution since favorable motions of the inner and outer boom would be chosen with a foresight of the following motion. As presented in Chapter 3.2.2, the application of global solutions is limited by the computing capacity of onboard control units. Furthermore, if the trajectory is planned spontaneously by the operator, the future motions will not be known at the instantaneous time step. Pre-calculated trajectories of common motions could provide a remedy to this problem. These would need to be stored on the onboard

control unit and could be retrieved by the operator.

6 Conclusion and Prospects

Conclusion

This thesis presents a novel approach to a power optimizing algorithm applied on a knuckle-boom crane. This algorithm enables an energy-saving control of the end-effector by solving the redundancy of the crane arm with respect to the volumetric flow rate and pressure of the hydraulic load sensing system.

An existing approach was given by a former thesis [24], addressing this problem, by the use of a weighted pseudoinverse solution. This thesis provides a functioning simulation model, which supplies an applicable test environment for the novel approach of this thesis. With the aim of an energy-saving solution, existing approaches to this problem are presented, distinguishing between on-line and off-line solutions. Due to limited computational capacity and the advantages of real-time capability, an on-line solution is chosen. Therefore, the kinematics of the knuckle-boom crane are investigated and the motion of the end-effector is expressed as a function of the hydraulic cylinder motion. This is done by coordinate transformations by applying Denavit Hartenberg notation. The redundancy of the crane arm is solved by a least-norm solution using the pseudoinverse formulation. Inspired by Cheng et al. [9], in use of the gradient projection method, the pseudoinverse solution is modified to a volumetric flow rate optimizing solution. This approach is extended to a power optimizing solution by considering the hydraulic pressure of each hydraulic cylinder. This is achieved, by including a feedback of the cylinder's pressure into the performance gradient of the gradient projection method. To increase the influence of the pressure feedback, an exponent is applied to the feedback. In order to enhance further energy savings, a hydraulic transformer is included in the pseudoinverse solution in a similar manner to [24]. This transformer exploits the potential energy of the inner and outer boom during contrary motions.

The volumetric flow rate optimizing algorithm from [9] and the power optimal solution designed in this thesis are tested and validated in a simulation model, by performing representative trajectories. The energy consumption due to the performance of the algorithms is compared for a conventional system and a system including the hydraulic transformer. As a reference condition, the least norm solution is chosen, which solves the redundancy by pseudoinverse solution. All algorithms contain a joint limit avoidance to obey the kinematic restrictions of the crane arm.

The volumetric flow rate optimizing algorithm performed poorer than the reference condition while testing on the energy optimization potential. Whereas the power optimizing algorithm successfully reduces the system energy up to 26.9 %. The hydraulic transformer improves the energy-saving potential of the algorithm for horizontal motions. In comparison to a conventional system with a regular least norm solution, up to 31.8 % more energy is saved by the HT system with a power optimizing algorithm. For vertical motions, the

